

Multidimensional Heteronuclear NMR Experiments

In order to study the structure and dynamics of proteins, the spectral resonances must be identified before the structural information and relaxation parameters can be utilized. This chapter addresses the general strategy and heteronuclear experiments required to achieve sequence-specific assignments of backbone and side-chain resonances. Practical aspects related to the experiments will also be discussed in detail.

Key questions to be addressed in the current chapter include:

1. How do the HSQC and HMQC experiments work?
2. How does the TROSY experiment work?
3. How does the IPAP-HSQC experiment work?
4. What are variants of these experiments used for?
5. What are the experiments necessary for backbone and side-chain assignments?
6. How is the magnetization transferred during each of the experiments in terms of product operators?
7. What types of information can be obtained from each experiment?
8. What are the typical procedures to set up these experiments?
9. What is the general strategy to obtain complete assignments using the above experiments?
10. How are the multidimensional NMR data processed?

5.1. TWO-DIMENSIONAL HETERONUCLEAR EXPERIMENTS

HSQC (heteronuclear single-quantum coherence) and HMQC (heteronuclear multi-quantum correlation) experiments (Mueller, 1979; Bodenhausen and Ruben, 1980; Bax *et al.*, 1990b; Hurd and John, 1991) are the basic building blocks of multidimensional experiments. In the experiments, the heteronuclear correlations via one-bond scalar couplings are obtained by observing the ^1H signals because ^1H is more sensitive relative to the heteronuclei. The relative sensitivity of a heteronuclear isotope to ^1H is defined as:

$$\rho_i = \frac{S_X}{S_{1\text{H}}} = \frac{N_X \gamma_X^3 I(I+1)}{N_{1\text{H}} \gamma_{1\text{H}}^3 \frac{1}{2}(\frac{1}{2}+1)} \quad (5.1)$$

in which S_X and S_{1H} are the signal-to-noise ratios of heteronucleus X and 1H , respectively, N is the number of the nucleus, which corresponds to the natural abundance of the nucleus, I is the nuclear spin quantum number, and γ is the gyromagnetic ratio. For equal numbers of spin- $\frac{1}{2}$ nuclei, the relative sensitivity to 1H is given by:

$$\rho_i = \left(\frac{\gamma_X}{\gamma_{1H}} \right)^3 \quad (5.2)$$

The relative sensitivities of ^{13}C and ^{15}N are approximately 1.6×10^{-2} and 1.0×10^{-3} , respectively. Therefore, the sensitivity is increased by observing 1H as in HSQC and HMQC, compared to observing the heteronuclei. These experiments are also the most routinely acquired proton-detected heteronuclear correlation experiments used in structural and dynamic studies of proteins. Understanding how the experiments work, how they are carried out, and what types of information can be obtained will certainly aid in the understanding of more complicated multidimensional experiments (see below).

5.1.1. HSQC and HMQC

The pulse sequence of HSQC (Figure 5.1) uses the INEPT (insensitive nuclei enhancement by polarization transfer) sequence to transfer proton magnetization into heteronuclear single-quantum coherence. After it is frequency labeled according to the heteronuclear

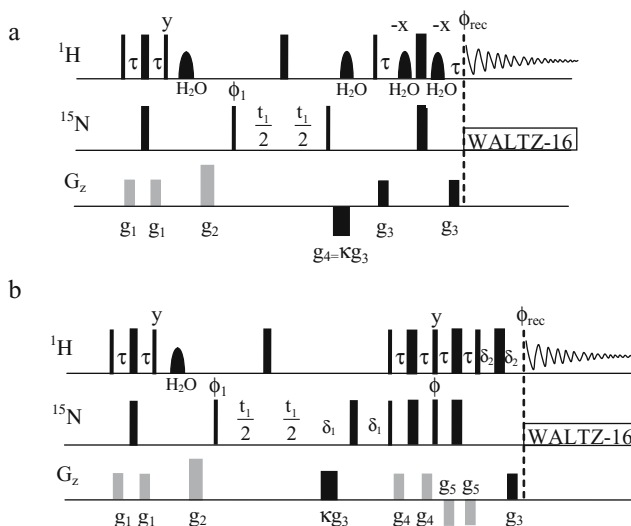


Figure 5.1. Pulse sequences for gradient HSQC experiments. (a) Water-flip-back using a 1 ms 90° Gaussian selective pulse is combined with the watergate sequence for solvent suppression. (b) A PEP sensitivity enhanced HSQC with water-flip-back is acquired for a pair of data sets by inverting the sign of κ and the phase of ϕ . For both pulse sequences, $\phi_1 = x - x + \text{States-TPPI}$, $\phi_{rec} = x - x$, and $k = \pm 10$, $\phi = \pm y$ for PEP. The phases of all other pulses are x . Delays τ are set to 2.7 ms, δ_1 is the pulse length of gradient pulse κg_3 , δ_2 for gradient g_3 . The black gradient pulses are used for coherence selection.

chemical shift during the following evolution period, the heteronuclear SQ coherence is transferred back into proton magnetization via the second INEPT sequence. The desired SQ coherence pathway is selected by the gradient pulses. The first gradient pulse dephases heteronuclear magnetization by producing a spatially dependent phase shift of $\phi_X = \gamma_X G_4$ at the end of the evolution period t_1 . After the magnetization is transferred back to the ^1H spins, the coupled coherence is refocused by G_3 according to the refocusing condition:

$$\pm\gamma_X G_4 - \gamma_H G_3 = 0 \quad \text{or} \quad G_4 = \pm \frac{\gamma_H}{\gamma_X} G_3 = \kappa G_3 \quad (5.3)$$

in which signs $+$ and $-$ produce P- and N-type spectra, respectively. Either type will give t_1 frequency discrimination type data with a phase twisted line shape as described in the COSY experiment. The value of κ is set to ± 10 and ± 4 for ^{15}N and ^{13}C heteronuclear correlation, respectively. The opposite sign of G_3 to G_4 is to avoid refocusing any magnetization that is dephased by G_4 . The selective pulse on water is to ensure the water magnetization is in the longitudinal direction during acquisition to avoid the effect of saturation transfer on amide proton signals. The gradient applied immediately after the selective pulse dephases the transverse magnetization of the residual water.

The magnetization during the gHSQC can be described by product operator analysis as shown for INEPT since the experiment utilizes an INEPT sequence to transfer coupled H^{N} and N coherence. Starting at $^1\text{H}^{\text{N}}$ (H) coupled with ^{15}N (N), the magnetization transfer pathway is represented using the product operators as follows:

$$\begin{aligned} & \text{H}_z \xrightarrow{\frac{\pi}{2} \text{H}_x} -\text{H}_y \\ & -\text{H}_y \xrightarrow{\tau \rightarrow \pi(\text{H}_x + \text{N}_x) \rightarrow \tau \rightarrow \frac{\pi}{2}(\text{H}_y + \text{N}_y)} -2\text{H}_z \text{N}_y \end{aligned} \quad (5.4)$$

(Proton magnetization is transferred to nitrogen in the first INEPT sequence. See section 1.12.2.3 for details.)

$$-2\text{H}_z \text{N}_y \xrightarrow{\frac{t_1}{2} \rightarrow \pi \text{H}_x \rightarrow \frac{t_1}{2}} 2\text{H}_z \text{N}_y \cos(\Omega_s t_1) - \text{H}_z \text{N}_x \sin(\Omega_s t_1) \quad (5.5)$$

(The magnetization is frequency labeled during the t_1 evolution period.)

$$\xrightarrow{\frac{\pi}{2}(\text{H}_x + \text{N}_x) \rightarrow \tau \rightarrow \pi(\text{H}_x + \text{N}_x) \rightarrow \tau} -\text{H}_x \cos(\Omega_s t_1) - 2\text{H}_y \text{N}_x \sin(\Omega_s t_1) \quad (5.6)$$

(The magnetization is transferred back to protons during reverse INEPT.) in which τ is set to $1/(4J_{\text{HN}})$. The 180° pulse on spin H in the middle of the t_1 period refocuses the coupling of spin H and N and hence removes the coupling J_{HN} in the F_1 dimension (^{15}N). Thus, the line shape on F_1 dimension does not include a contribution from J_{IS} coupling. The term $\text{H}_y \text{N}_x$ represents multi-quantum coherence that is unobservable magnetization.

5.1.2. HSQC Experiment Setup

A water suppression sequence such as water-flip-back is usually integrated into a gradient HSQC pulse sequence (Figure 5.1). The ^1H 90° pulse is calibrated first after the probe is tuned. The transmitter carrier frequency (^1H) is then calibrated by setting the offset frequency on the water resonance and acquiring a PRESAT experiment with the transmitter offset frequency arrayed over ± 3 Hz in 0.5 Hz steps (see previous chapter). A water-selective shaped 90° pulse is calibrated by arraying the fine power of the pulse (refer to the section on shaped pulse). The ^{15}N decoupler offset frequency is set to 118 ppm, which should be used for all ^{15}N double- and triple-resonance experiments. Timing parameters include a delay τ of 2.65 ms, a relaxation delay time of 1 s, and an acquisition time of 64 ms. The first FID of HSQC is recorded for a test run to optimize the receiver gain for better sensitivity. The dead time and receiver phase are adjusted to obtain a phase-correct spectrum without phase correction. Two-dimensional data are collected with 128 increments.

In the ^1H dimension, the data size is doubled with mirror image linear prediction followed by apodization with a 60° shifted square sine-bell function, zero filling to 2048 complex points, and Fourier transformation. If the phase parameters are not optimized before acquisition, they are obtained using the first FID of the 2D data. Since only the amide protons are observed in the experiment, the upfield half of the ^1H spectrum (frequency range lower than 6 ppm) is eliminated before processing the ^{15}N dimension. After being transposed, the interferogram is processed in the same way as the ^1H dimension except with zero filling to 512 complex points.

A phase sensitive gradient HSQC can be acquired using States, TPPI, or States-TPPI methods to obtain a pure absorptive spectrum in both dimensions. It can also be acquired with a sensitivity enhanced method (also known as PEP, preservation of equivalent pathway; and COS for coherence order selective) to improve the sensitivity of the experiment by a factor of $2^{1/2}$ over the conventional gradient HSQC.

Water suppression schemes such as water-flip-back and Watergate can be implemented into the HSQC sequence to efficiently suppress water (Figure 5.1b). The water-flip-back uses a water selective pulse after the first INEPT to bring the water magnetization back to the z axis. The water magnetization remains along the z axis during reverse INEPT and WATERGATE, while only the residual water magnetization resulting from pulse imperfection is efficiently dephased by the WATERGATE sequence. Utilization of the flip-back pulse prevents dephasing the majority of the water magnetization so as to avoid saturation transfer. As a result, the sensitivity is improved by 10–20% over the sequence without the water-flip-back pulse (Grzesiek and Bax, 1993).

5.1.3. Sensitivity Enhanced HSQC by PEP

The PEP sensitivity enhancement method has been incorporated into the HSQC sequence to improve sensitivity without increasing the experimental time (Cavanagh *et al.*, 1991; Kay *et al.*, 1992; Akke *et al.*, 1994). In conventional HSQC, reverse INEPT transfers the magnetization back to ^1H [see equations (5.4)–(5.6)]:

$$-2\text{H}_z\text{N}_y \xrightarrow{t_1 \rightarrow \frac{\pi}{2}(\text{H}_x + \text{N}_x) \rightarrow \tau \rightarrow \pi(\text{H}_x + \text{N}_x) \rightarrow \tau} -\text{H}_x \cos(\Omega_N t_1) - 2\text{H}_y\text{N}_x \sin(\Omega_N t_1) \quad (5.7)$$

The second term represents multiple-quantum coherence that is not observable. Therefore, only the cosine component of the t_1 evolution will be detected. A sensitivity enhanced HSQC using the PEP method (Figure 5.1b) allows the detection of both components of the coherence.

The last period after the reversed INEPT in the pulse sequence is for PEP sensitivity enhancement, in which the two terms of the coherence can be considered separately. The first FID is acquired with $\phi = x$ and $\kappa = 10$ and the second one is recorded with both the phase ϕ and gradient κ inverted (i.e. $-x$ and -10 , respectively). During PEP, the coherence for the first FID yields:

$$\begin{aligned}
 -H_x \cos(\Omega_N t_1) - 2H_y N_x \sin(\Omega_N t_1) &\xrightarrow{\frac{\pi}{2}(H_y + N_y)} H_z \cos(\Omega_N t_1) + 2H_y N_z \sin(\Omega_N t_1) \\
 &\xrightarrow{\tau \rightarrow \pi(H_x + N_x) \rightarrow \tau} -H_z \cos(\Omega_N t_1) - H_x \sin(\Omega_N t_1) \\
 &\xrightarrow{\frac{\pi}{2} H_x} H_y \cos(\Omega_N t_1) - H_x \sin(\Omega_N t_1) \quad (5.8)
 \end{aligned}$$

The second FID is obtained by inverting phase ϕ and the sign of gradient factor κ :

$$\begin{aligned}
 -H_x \cos(\Omega_N t_1) - 2H_y N_x \sin(\Omega_N t_1) &\xrightarrow{\frac{\pi}{2}(H_y - N_y)} H_z \cos(\Omega_N t_1) - 2H_y N_z \sin(\Omega_N t_1) \\
 &\xrightarrow{\tau \rightarrow \pi(H_x + N_x) \rightarrow \tau} -H_z \cos(\Omega_N t_1) + H_x \sin(\Omega_N t_1) \\
 &\xrightarrow{\frac{\pi}{2} H_x} H_y \cos(\Omega_N t_1) + H_x \sin(\Omega_N t_1) \quad (5.9)
 \end{aligned}$$

Therefore, the two FIDs acquired and stored in separated memory locations in the same data are given by:

$$\text{FID1} \propto H_y \cos(\Omega_N t_1) - H_x \sin(\Omega_N t_1) \quad (5.10)$$

$$\text{FID2} \propto H_y \cos(\Omega_N t_1) + H_x \sin(\Omega_N t_1) \quad (5.11)$$

Addition of the two FIDs gives rise to a data set that contains observable magnetization described by:

$$2H_y \cos(\Omega_N t_1) \quad (5.12)$$

Similarly, subtraction of the two FIDs ($\text{FID}_2 - \text{FID}_1$) yields a second data set:

$$2H_x \sin(\Omega_N t_1) \quad (5.13)$$

The two PEP data sets can be processed to obtain separate 2D spectra. The spectra are then combined to form a single spectrum with pure absorptive line shapes on both dimensions. Because the noise is increased by a factor of $\sqrt{2}$ and the signal intensity is increased by 2 after the spectral combination, the combined spectrum increases the sensitivity by a maximum of $\sqrt{2}$ compared to that in the conventional gradient HSQC spectrum without considering the relaxation factor (Palmer *et al.*, 1991; Kay *et al.*, 1992; Cavanagh and Rance, 1993; Schleucher *et al.*, 1994; Muhandiran and Kay, 1994). For a ^1H - ^{13}C HSQC experiment, the identical result will be obtained by replacing operator N with C for ^{13}C spins.

The water signal can be suppressed during the PEP sequence. In a conventional gradient enhanced HSQC experiment, the water magnetization is fully dephased by the gradient echo immediately before the data acquisition. This causes reduction of NH magnetization through saturation transfer. In an seHSQC experiment, application of a selective water pulse combined with a two-step phase cycle for the ^1H pulse ensures that the water magnetization stays along the z axis prior to the acquisition period while the residual water is suppressed during dephasing by the gradient echo pulses. Since the saturation transfer is minimized and both the echo and anti-echo coherences are selected in the experiment, the sensitivity is improved in flip-back seHSQC compared to the conventional gradient phase sensitive HSQC in which quadrature detection in the F_1 dimension is obtained by using gradients to generate pure absorption spectra.

5.1.4. Setup of an seHSQC Experiment

The general procedure to setup experiments for aqueous samples includes tuning the probe for all three channels in the order of ^{15}N , ^{13}C , and then the ^1H channel; calibrating the 90° ^1H pulse; finding the resonance frequency of water; and calibrating the selective 90° pulse on water. The ^{15}N and ^{13}C pulses do not require recalibration for every experiment as long as they are calibrated regularly and the probe is well-tuned. The data are acquired with 1024 t_2 and 128 t_1 complex points. The initial t_1 value is set according to

$$t_1(0) = \frac{1}{2\text{SW}} - \text{pw}_{180(\text{H})} - \frac{4\text{pw}_{90(\text{N})}}{\pi} \quad (5.14)$$

whereas for CT-HSQC, the initial t_1 is chosen by

$$t_1(0) = \frac{1}{2\text{SW}} \quad (5.15)$$

5.1.5. HMQC

Shown in Figure 5.2a is an HMQC pulse sequence. The magnetization during the experiment can be described by product operator analysis. Starting at $^1\text{H}^{\text{C}}$ (H) coupled with ^{13}C (C), the magnetization transfer pathway is represented using the product operators as follows:

$$\text{H}_z \xrightarrow{\frac{\pi}{2}\text{H}_x} -\text{H}_y \xrightarrow{\tau} -\text{H}_y \cos(\pi J_{\text{HC}}\tau) + 2\text{H}_x\text{C}_z \sin(\pi J_{\text{HC}}\tau) \quad (5.16)$$

Delay τ is set to $1/(2J_{\text{HC}})$ to maximize the anti-phase (AP) coherence. The multiple-quantum coherence is generated by the 90° carbon pulse and evolves during t_1 time:

$$2\text{H}_x\text{C}_z \xrightarrow{\frac{\pi}{2}\text{C}_x} -2\text{H}_x\text{C}_y \xrightarrow{\frac{t_1}{2} \rightarrow \pi\text{H}_x \rightarrow \frac{t_1}{2}} -2\text{H}_x\text{C}_y \cos(\Omega_{\text{C}}t_1) + 2\text{H}_x\text{C}_x \sin(\Omega_{\text{C}}t_1) \quad (5.17)$$

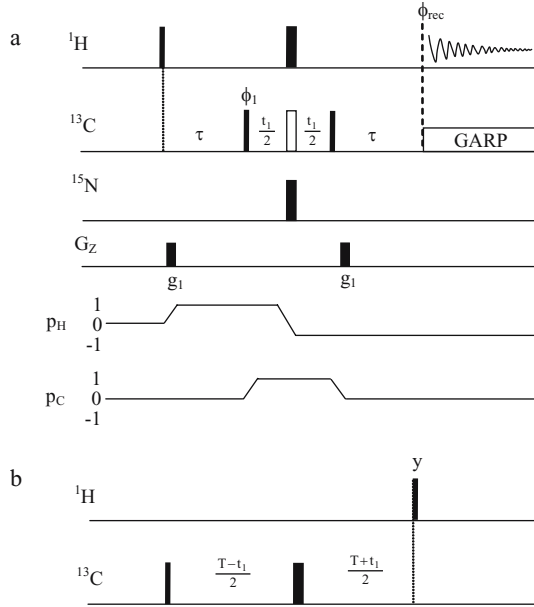


Figure 5.2. Pulse sequence for HMQC experiments. The 90° (narrow bars) and 180° (wider bars) are x phase except as indicated. (a) Conventional HMQC with the coherence transfer pathways shown below the pulse sequence. The open 180° pulse is a $^{13}\text{C}^\alpha$ - or $^{13}\text{C}^\beta$ -selective pulse, which can be turned on for decoupling $^{13}\text{C}^\alpha$ - $^{13}\text{C}^\beta$ coupling in the t_1 dimension since the frequency bands are well-separated with the exception of Gly, Ser, and Thr residues (McCoy, 1995; Matsuo *et al.*, 1996). Phase $\phi_1 = x, -x, +$ States-TPPI and $\phi_{\text{rec}} = x, -x$. Delay $\tau = 1/2J_{\text{CH}}$. Gradients are applied with duration of 0.5 ms and amplitude of $g_1 = 10 \text{ G cm}^{-1}$. (b) Constant-time element (Ernst *et al.*, 1987).

The 180° ^1H pulse in the middle of t_1 refocuses the evolution of the ^1H chemical shift during the t_1 period and during the τ period. Therefore, the magnetization of ^1H does not evolve. In addition, the heteronuclear scalar coupling does not affect the evolution of the multiple-quantum coherence $H_x C_y$ during t_1 . As a result, the only evolution occurring during t_1 is at the ^{13}C chemical shift frequency. The multiple-quantum coherence is converted into observable single-quantum magnetization by the ^{13}C 90° pulse combining with delay τ , while the zero-quantum term $H_x C_x$ will not produce observable coherence:

$$-2H_x C_y \cos(\Omega_C t_1) \xrightarrow{\frac{\pi}{2} C_x} -2H_x C_z \cos(\Omega_C t_1) \xrightarrow{\tau} -H_y \cos(\Omega_C t_1) \quad (5.18)$$

In summary,

$$H_z \xrightarrow{\frac{\pi}{2} H_x} -H_y \xrightarrow{\text{HMQC-type}} -H_y \cos(\Omega_C t_1) \quad (5.19)$$

The above product operator treatment does not include the homonuclear scalar coupling between protons and between ^{13}C carbons, which also evolves during the t_1 period of ^1H - ^{13}C HMQC. As a result, the F_1 dimension has the ^{13}C - ^{13}C scalar coupled multiplets as well as the contribution from ^1H - ^1H homonuclear coupling.

A constant time evolution period (Figure 5.2b) can be used to obtain F_1 decoupled spectra (Ernst *et al.*, 1987). In addition, recent studies have indicated that the relaxation rate of the ^1H – ^{13}C multiple-quantum coherence is much slower than that of ^1H – ^{13}C single-quantum coherence for nonaromatic methane sites in ^{13}C labeled protein and in nucleic acids at a slow tumbling limit. This property has been utilized to obtain better sensitivity in CT HMQC-type experiments than in CT HSQC-type experiments. During the CT evolution period, the homonuclear scalar coupling J_{CC} evolves for a period of $(T - t_1)/2 + (T + t_1)/2 = T$. Therefore, after the t_1 evolution period the magnetization in Equation (5.17) has a form of:

$$-2\text{H}_x\text{C}_y \xrightarrow{\frac{T-t_1}{2} \rightarrow \pi\text{H}_x \rightarrow \frac{T+t_1}{2}} [-2\text{H}_x\text{C}_y \cos(\Omega_{\text{C}}t_1) + 2\text{H}_x\text{C}_x \sin(\Omega_{\text{C}}t_1)] \cos(\pi J_{\text{CC}}T) \quad (5.20)$$

By setting the delay T to $1/(2J_{\text{CC}})$, the effect of J_{CC} can be removed.

5.1.6. IPAP HSQC

The IPAP (in-phase anti-phase) HSQC experiment is used to measure the residual dipolar coupling between amide ^1H and ^{15}N spins (Ottiger *et al.*, 1998). The experiment records two HSQC data sets, one of which yields IP doublets after Fourier transformation while the other gives AP doublets. Addition and subtraction of the spectra produce a pair of individual spectra each containing one of the doublet components. The coherence transfer during the pulse sequence can be described by product operators. The first ^{15}N 90° combined with the gradient pulse is used to ensure the initial magnetization originates only from amide proton spins. After the first INEPT transfer, the evolution of the ^1H – ^{15}N scalar coupling and ^{15}N chemical shift during the t_1 evolution period is given by (Figure 5.3):

$$\text{H}_z \xrightarrow{\frac{\pi}{2}\text{H}_x \rightarrow \tau \rightarrow \pi(\text{H}_x + \text{N}_x) \rightarrow \tau \rightarrow \frac{\pi}{2}(\text{H}_y + \text{N}_x)} 2\text{H}_z\text{N}_y \quad (\text{First INEPT}) \quad (5.21)$$

$$\begin{aligned} 2\text{H}_z\text{N}_y &\xrightarrow{t_1} 2\text{H}_z\text{N}_y \cos(\Omega_{\text{N}}t_1) \cos(\pi J_{\text{HN}}t_1) \quad (t_1 \text{ evolution period}) \\ &\quad - 2\text{H}_z\text{N}_x \sin(\Omega_{\text{N}}t_1) \cos(\pi J_{\text{HN}}t_1) + \text{IP} \end{aligned} \quad (5.22)$$

in which term IP contains only IP coherence N_y and N_x with the coefficients, which cannot be converted into observable magnetization at the beginning of the acquisition. Therefore, the IP term is omitted during the following transfer path. For the first data set, the coherence transferred in the same path as for conventional HSQC is given by:

$$\begin{aligned} &2\text{H}_z\text{N}_y \cos(\Omega_{\text{N}}t_1) \cos(\pi J_{\text{HN}}t_1) - 2\text{H}_z\text{N}_x \sin(\Omega_{\text{N}}t_1) \cos(\pi J_{\text{HN}}t_1) \\ &\xrightarrow{\frac{\pi}{2}(\text{H}_x + \text{N}_x)} -\text{H}_y\text{N}_z \cos(\Omega_{\text{N}}t_1) \cos(\pi J_{\text{HN}}t_1) + 2\text{H}_y\text{N}_x \sin(\Omega_{\text{N}}t_1) \cos(\pi J_{\text{HN}}t_1) \\ &\xrightarrow{\tau \rightarrow \pi(\text{H}_x + \text{N}_x) \rightarrow \tau} \text{H}_x \cos(\Omega_{\text{N}}t_1) \cos(\pi J_{\text{HN}}t_1) \end{aligned} \quad (5.23)$$

in which $\tau = 1/(4J_{\text{HN}})$ and the multiple-quantum term H_yN_x cannot be converted to observable magnetization and thus is omitted.

The second data set is collected by inserting an ^{15}N refocusing period before the evolution time to obtain AP doublets. The magnetization after the first INEPT transfer with phase ϕ_2

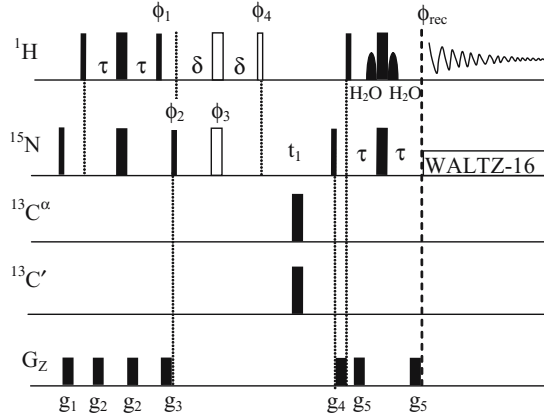


Figure 5.3. Pulse sequence for IPAP [^1H , ^{15}N] HSQC experiment. The sequence element δ - 180° ($^1\text{H}/^{15}\text{N}$)- δ - 90° (open pulses) is only used in the experiment for generating the anti-phase (AP) spectrum and is omitted for generating the in-phase (IP) spectrum. The 90° (narrow bars) and 180° (wider bars) are x phase except $\phi_1 = -y, y$; $\phi_2 = 2(x), 2(-x), +$ States-TPPI for IP; $\phi_2 = 2(-y), 2(y), +$ States-TPPI for AP; $\phi_3 = 4(x), 4(y), 4(-x), 4(-y), +$ States-TPPI; $\phi_4 = 8(x), 8(-x)$; $\phi_{\text{rec}} = x, 2(-x), x$ for IP; $\phi_{\text{rec}} = x, 2(-x), x, -x, 2(x), -x$ for AP. Delays $\tau = 2.5$ ms, $\delta = 2.65$ ms. The gradients are sine-bell shaped with an amplitude of 25 G cm^{-1} and durations of 2, 0.4, 2, 1, and 0.4 ms for g_1, g_2, g_3, g_4 , and g_5 , respectively. IP and AP spectra are recorded in an interleaved manner (from Ottiger *et al.*, 1998).

decreased by 90° is given by:

$$\text{H}_z \xrightarrow{\frac{\pi}{2} \text{H}_x \rightarrow \tau \rightarrow \pi(\text{H}_x + \text{N}_x) \rightarrow \tau \rightarrow \frac{\pi}{2}(\text{H}_y - \text{N}_y)} 2\text{H}_z\text{N}_x \quad (5.24)$$

The coherence after the ^{15}N refocusing period is described by:

$$2\text{H}_z\text{N}_x \xrightarrow{\delta \rightarrow \pi(\text{H}_x + \text{N}_x) \rightarrow \delta \rightarrow \frac{\pi}{2} \text{H}_x} 2\text{H}_y\text{N}_x \cos(2\pi J_{\text{HN}}\delta) - \text{N}_y \sin(2\pi J_{\text{HN}}\delta) \quad (5.25)$$

in which the delay δ is optimized to $1/4J_{\text{NH}}$, approximately 2.65 ms. Ignoring the multiple-quantum term, the evolution of scalar coupling J_{HN} and ^{15}N chemical shift yields:

$$\begin{aligned} -\text{N}_y \sin(2\pi J_{\text{HN}}\delta) &\xrightarrow{t_1} 2\text{H}_z\text{N}_x \cos(\Omega_{\text{N}}t_1) \sin(\pi J_{\text{HN}}t_1) + 2\text{H}_z\text{N}_y \sin(\Omega_{\text{N}}t_1) \sin(\pi J_{\text{HN}}t_1) + \text{IP} \\ &\xrightarrow{\frac{\pi}{2}(\text{H}_x + \text{N}_x)} -2\text{H}_y\text{N}_x \cos(\Omega_{\text{N}}t_1) \sin(\pi J_{\text{HN}}t_1) - 2\text{H}_y\text{N}_z \sin(\Omega_{\text{N}}t_1) \sin(\pi J_{\text{HN}}t_1) \\ &\xrightarrow{\tau \rightarrow \pi(\text{H}_x + \text{N}_x) \rightarrow \tau} \text{H}_x \sin(\Omega_{\text{N}}t_1) \sin(\pi J_{\text{HN}}t_1) \end{aligned} \quad (5.26)$$

Addition of the two FIDs produces:

$$\text{H}_x \cos(\Omega_{\text{N}}t_1) \cos(\pi J_{\text{HN}}t_1) + \text{H}_x \sin(\Omega_{\text{N}}t_1) \sin(\pi J_{\text{HN}}t_1) = \text{H}_x \cos[(\Omega_{\text{N}} - \pi J_{\text{HN}})t_1] \quad (5.27)$$

according to $\cos(\alpha)\cos(\beta) + \sin(\alpha)\sin(\beta) = \cos(\alpha - \beta)$, whereas subtraction of the data gives:

$$H_x \cos(\Omega_N t_1) \cos(\pi J_{HN} t_1) - H_x \sin(\Omega_N t_1) \sin(\pi J_{HN} t_1) = H_x \cos[(\Omega_N + \pi J_{HN})t_1] \quad (5.28)$$

because $\cos(\alpha)\cos(\beta) - \sin(\alpha)\sin(\beta) = \cos(\alpha + \beta)$. Fourier transformation of the combined data sets generates individual spectra with one of the doublets at either $\Omega_N - \pi J_{HN}$ or $\Omega_N + \pi J_{HN}$. The above product operator treatment does not include the effect of relaxation that causes the signal loss in the second FID during the 2δ period, which is a factor of $e^{2\delta/T_2}$. Deviation of J_{HN} from the selected value of δ also causes a signal loss, but the loss is identical for both IP and AP spectra. Thus, it is necessary to multiply a scaling factor before addition or subtraction, which can be adjusted during data processing. The quadrature detection in the t_1 dimension is achieved by the States–TPPI phase mode, because the IPAP does not provide frequency discrimination in the t_1 dimension as shown above. By altering the phase of the first ^{15}N 90° pulse (IP) and both the first ^{15}N 90° pulse and the ^{15}N 180° pulse during 2δ period (AP) in the States–TPPI manner, the two phase-sensitive IP and AP FIDs can be obtained:

$$H_x \cos(\pi J_{HN} t_1) e^{-i\Omega_N t_1} \quad (5.29)$$

$$iH_x \sin(\pi J_{HN} t_1) e^{-i\Omega_N t_1} \quad (5.30)$$

The data obtained after addition and subtraction are given by:

$$H_x e^{-i(\Omega_N - \pi J_{HN})t_1} \quad (5.31)$$

$$H_x e^{-i(\Omega_N + \pi J_{HN})t_1} \quad (5.32)$$

The IPAP method can also be implemented in triple resonance experiments to resolve the overlapped signals.

5.1.7. SQ-TROSY

The TROSY (transverse relaxation optimized spectroscopy) experiment utilizes the interference effect of cross-correlated relaxations caused by CSA and dipolar interaction on the T_2 relaxation rate at the individual multiplet components to reduce the line width of heteronuclear correlation spectra (Pervushin *et al.*, 1997). For a weakly coupled two spin- $\frac{1}{2}$ system isolated from other spins in a protein molecule, T_2 relaxation of the spin system is dominated by the CSA of each individual spin and the DD coupling between the two spins. The CSA has the same effect on the T_2 relaxation of all multiplet components, while the effect of DD coupling on the T_2 relaxation of the resonances from the β transitions is opposite to the effect from CSA. This interference effect from CSA and DD coupling leads to different T_2 relaxations for the doublet peaks of the individual spins in the spin system. When the orientations of the two interactions are approximately collinear and their magnitudes are comparable, the line widths originating from the β transitions are reduced and those from the α transitions are broadened (Figure 1.23; Pervushin *et al.*, 1997).

The interference effect can be well-understood by considering the relaxation matrix containing single-quantum transition operators. For macromolecules in aqueous solution, the

isotropic motion of the molecules is in the slow-tumbling limit. Only the spectral density, $J(0)$, contributes significantly to the relaxation rate. The change of the magnetization corresponding to the transitions as a function of time can be represented by the first-order relaxation matrix (Sørensen *et al.*, 1983; Ernst *et al.*, 1987; Pervushin *et al.*, 1997):

$$\frac{d}{dt} \begin{bmatrix} I_{13}^{\pm} \\ I_{24}^{\pm} \\ S_{12}^{\pm} \\ S_{34}^{\pm} \end{bmatrix} = - \left\{ i \begin{bmatrix} \pm \omega_I^{13} \\ \pm \omega_I^{24} \\ \pm \omega_S^{12} \\ \pm \omega_S^{34} \end{bmatrix} + 4J(0) \begin{bmatrix} p^2 - 2C_{p,\delta_I} p \delta_I + \delta_I^2 \\ p^2 + 2C_{p,\delta_I} p \delta_I + \delta_I^2 \\ p^2 - 2C_{p,\delta_S} p \delta_S + \delta_S^2 \\ p^2 + 2C_{p,\delta_S} p \delta_S + \delta_S^2 \end{bmatrix} \right\} \begin{bmatrix} I_{13}^{\pm} \\ I_{24}^{\pm} \\ S_{12}^{\pm} \\ S_{34}^{\pm} \end{bmatrix} \quad (5.33)$$

in which I_{ij}^{\pm} and S_{ij}^{\pm} are the magnetization of spins I and S corresponding to the single-quantum transitions $i \leftrightarrow j$ in the standard energy diagram (Figure 1.19) with the corresponding resonance frequencies:

$$\begin{aligned} I_{13}^{\pm} &\Rightarrow \text{transition } 1 \leftrightarrow 3, & \omega_I^{13} &= \omega_I + \pi J_{IS} \\ I_{24}^{\pm} &\Rightarrow \text{transition } 2 \leftrightarrow 4, & \omega_I^{24} &= \omega_I - \pi J_{IS} \\ S_{12}^{\pm} &\Rightarrow \text{transition } 1 \leftrightarrow 2, & \omega_S^{12} &= \omega_I - \pi J_{IS} \\ S_{34}^{\pm} &\Rightarrow \text{transition } 3 \leftrightarrow 4, & \omega_S^{34} &= \omega_S + \pi J_{IS} \end{aligned} \quad (5.34)$$

$J(0)$ is the spectral density function at the zero-frequency, $C_{kl} = \frac{1}{2}(3 \cos^2 \Theta_{kl} - 1)$ and Θ_{kl} is the angle between the tensor axes of the interaction k and l , and p , δ_I , and δ_S are given by:

$$p = \frac{1}{2\sqrt{2}} \frac{\gamma_I \gamma_S \hbar}{r_{IS}^3}, \quad \delta_I = \frac{\gamma_I B_0 \Delta\sigma_I}{3\sqrt{2}}, \quad \delta_S = \frac{\gamma_S B_0 \Delta\sigma_S}{3\sqrt{2}} \quad (5.35)$$

in which γ_I and γ_S are the gyromagnetic ratios of spin I and S , respectively, \hbar is Plank's constant divided by 2π , r_{IS} is the distance between the two spins, B_0 is the magnetic field strength, $\Delta\sigma_I$ and $\Delta\sigma_S$ are the chemical shift difference between the axial and perpendicular principle components of the axially symmetric CSA of spin I and S , respectively. Equation (5.33) tells us that if the magnitudes of CSA and DD coupling are comparable ($p \approx -\delta_S$ and $p \approx -\delta_I$ for $I = {}^1\text{H}$ and $S = {}^{15}\text{N}$), and the principal symmetric axis of the CSA tensor and the bond vector r_{IS} are approximately collinear, such as in the case of the backbone amide NH moiety of the proteins, the line widths at the resonance frequencies ω_I^{24} and ω_S^{34} are narrower than the other two due to the slow transverse relaxation even for large size proteins (Pervushin *et al.*, 1999). For backbone NH, $\Delta\sigma_{\text{H}} = 15$ ppm, $\Theta_{p,\delta_{\text{H}}} = 10^\circ$ (Gerald *et al.*, 1993), $\Delta\sigma_{\text{N}} = -156$ ppm, and $\Theta_{p,\delta_{\text{N}}} = 17^\circ$ (Teng and Cross, 1989). Therefore, both ${}^1\text{H}$ and ${}^{15}\text{N}$ CSA tensors are almost axial symmetric and nearly collinear with the DD vector (the ${}^1\text{H}$ bond). It has been estimated using the above values that the transverse relaxation effect at ${}^1\text{H}$ frequencies can be completely cancelled for one of the four multiplet components when the magnetic field strength is near 1 GHz (Pervushin *et al.*, 1997).

Shown in Figure 5.4 is the water-flip-back ${}^1\text{H}/{}^{15}\text{N}$ TROSY pulse sequence. The experiment specially correlates the ${}^{15}\text{N}$ $4 \rightarrow 3$ transition with ${}^1\text{H}$ $4 \rightarrow 2$ through the single-quantum transition (SQ-TROSY; Pervushin *et al.*, 1999). Saturation of the water magnetization is avoided during the experiment by the water-flip-back pulses at the beginning of the pulse

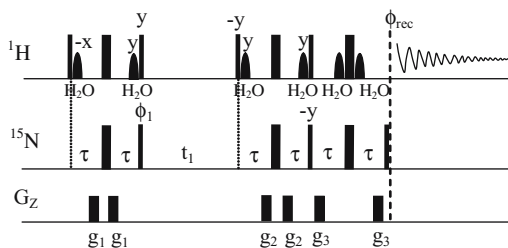


Figure 5.4. Pulse sequence for TROSY experiment. The 90° (narrow bars) and 180° (wider bars) are x phase except $\phi_1 = y, x, +$ States–TPPI, $\phi_{\text{rec}} = y, -x$ and others as indicated. The selective H_2O 90° pulses (shaped) are used to avoid the saturation of water by retaining water magnetization along z axis during the experiment. The delay $\tau = 2.7$ ms. Gradients are applied with a duration of 1 ms and amplitudes $g_1 = 30 \text{ G cm}^{-1}$, $g_2 = 40 \text{ G cm}^{-1}$, and $g_3 = 48 \text{ G cm}^{-1}$.

sequence. The selective pulses on the water resonance during the first INEPT sequence are used to keep the water magnetization on the z axis during the t_1 evolution period. The two water selective pulses during the SQ polarization transfer element ensure the water magnetization is on the z axis immediately before acquisition, resulting in a minimal saturation transfer from water to the exchangeable NHs. The watergate element at the end of the pulse sequence is used to suppress the residual transverse water magnetization before acquisition.

5.2. OVERVIEW OF TRIPLE-RESONANCE EXPERIMENTS

The homonuclear NOE is a widely utilized technique in various types of calculation methods, such as distance geometry, restrained molecular dynamics (or simulated annealing), and variable target function methods in structural characterization of proteins based on the information on approximate distances between protons obtained in NOESY or ROESY experiments. Before the information can be used, the origin of each resonance in the NMR spectrum must be linked to a nucleus in the molecular sequence. The process is called sequence-specific assignment. In order to obtain a high resolution structure, it is necessary to complete the assignment for a sufficient number of atoms in the sequence. Frequently, the heteronuclear isotopes (^{15}N and/or ^{13}C) are also used to establish sequential assignment as well as to increase the spectral resolution by spreading ^1H resonances on the heteronuclear dimensions so that the degeneracy of ^1H resonances can be reduced. Two types of nuclear interactions are used in NMR spectra for the assignment of the chemical shifts of the nuclei: through-bond interaction—scalar coupling, and through-space interaction—dipolar coupling via NOE.

For homonuclear correlations, the sequential assignments must be done by the inter-residue backbone NOEs due to the near-zero ^1H four bond scalar coupling. However, an inter-residue NOE may not occur between sequential correlations. In addition, for large proteins (M.W. > 10 kDa) for which resonance degeneracy becomes severe, it is extremely difficult to assign the resonances even if ^{15}N edited experiments are employed. Consequently, it is necessary to make use of ^{13}C isotopes in the sequence-specific assignment. With the current availability of ^{13}C glucose, which is the most frequently used ^{13}C source in the preparation of ^{13}C labeled proteins (details in Chapter 3), the cost of ^{13}C labeling has decreased to an affordable level, and it promises to be even less expensive in the future as isotopic labeling

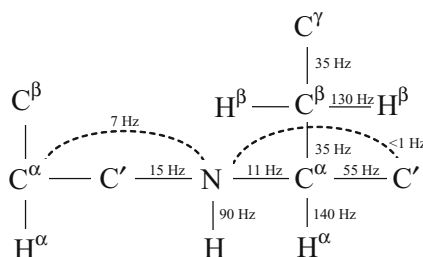


Figure 5.5. J coupling constants between ^1H , ^{15}N , and ^{13}C along a polypeptide chain as used in triple-resonance NMR experiments for resonance assignments.

is becoming a standard procedure in NMR sample preparation for structure study. One of the advantages of heteronuclear isotopic labeling is the much larger scalar couplings than those between protons (Figure 5.5). The larger scalar coupling constant means that the magnetization transfer between heteronuclear spins is more efficient, resulting in more intense cross-peaks. By introducing a ^{13}C frequency dimension, the resonance ambiguity can be further reduced with higher spectral resolution, and hence the resonance assignment is significantly simplified.

A large number of triple resonance experiments have been developed and optimized for structure determination of proteins using heteronuclear multidimensional NMR spectroscopy. These experiments make full use of one- and two-bond heteronuclear scalar couplings to correlate the backbone and side-chain ^1H , ^{15}N , and ^{13}C spins of isotope labeled proteins. Because the 1J and 2J couplings (shown in Figure 5.5) generally are relatively large compared to the spectral line width, and independent of conformation, the coherence transfers through these couplings can efficiently compete with the loss of magnetization caused by short transverse relaxation times during the experiment. The nomenclature used for triple-resonance experiments is based on the coherence transfer pathway in the experiment. The name of an experiment is formed by the spins involved in the coherence transfer in the order following the transfer pathway. Spins are given in parentheses if their chemical shifts do not evolve. The name is formed only by the first half of the coherence transfer when the magnetization of the proton spin is transferred to neighboring spins and then back to the proton by the same pathway. This type of experiment is called “out and back.” For instance, in a 3D triple-resonance “out and back” type experiment, the magnetization of an amide proton (H^N) is transferred to the C^α carbon (CA) via the amide nitrogen (N) and then back to the amide proton via the amide nitrogen, and hence it is called HNCA. If the magnetization is transferred further from C^α to carbonyl carbon C' (CO) and a chemical shift of C' evolves instead of C^α , the experiment is named HN(CA)CO. The parentheses reflect that the chemical shifts of C^α carbons involved in the magnetization transfer do not evolve during the experiment.

Although a variety of triple resonance experiments are available, only a certain number of experiments are frequently used to obtain backbone and side-chain assignments. Scalar couplings used in the experiments are summarized in Figure 5.5. The combination of the 3D experiments HNCA (Ikura *et al.*, 1990a,b; Kay *et al.*, 1990; Grzesiek and Bax, 1992c) and HN(CO)CA (Ikura *et al.*, 1990a,b; Kay *et al.*, 1991; Grzesiek and Bax, 1992c) can be used to establish backbone sequential connectivities by connecting the resonance frequencies of spins with those of preceding residue. HN(CO)CA provides correlations of H_i^N and N_i of residue i with C_{i-1}^α chemical shifts of the preceding residue $i - 1$, whereas HNCA correlates the

chemical shifts of H_i^N and N_i with both C_i^α and C_{i-1}^α because the scalar coupling $^2J_{NC_\alpha}$ of 7 Hz has a similar size to $^1J_{NC_\alpha}$ of 11 Hz. The correlation between N and C^α within a residue is not observed in HN(CO)CA due to the very weak $^2J_{NC'}$ (<1 Hz). These experiments are relatively sensitive and usually yield an excellent signal-to-noise ratio. Another pair of 3D experiments, CBCANH and CBCA(CO)NH (Grzesiek and Bax, 1992a,b), are used to extend the connectivities from the backbone to C^β , which provides useful information on the type of amino acids. Assignment of C^α and C^β will also be used to establish side-chain connectivity in addition to the backbone assignment. For proteins with more than 130 residues, ambiguities in assignment sometimes still remain based on the data obtained from the above four experiments. Then, a pair of experiments, HNCO (Ikura *et al.*, 1990a; Grzesiek and Bax, 1992c) and HN(CA)CO (Clubb *et al.*, 1992; Kay *et al.*, 1994; Engelke and Rüterjans, 1995), which spread H^N -N correlations into C' chemical shifts, are generally sufficient to completely resolve the spectral overlap. In practice, the six experiments will provide the backbone assignments. Since these six experiments are the most commonly used for backbone assignments, they will be discussed in detail in the following sections. It has been noted that HN(CA)CO has the lowest sensitivity compared to the other five experiments. Therefore, it may require more transients to achieve a sizable S/N for spectral analysis and sometimes a subset of cross-peaks may not be observable. However, with the use of a cryogenic probe, the problem of low sensitivity for HN(CA)CO can be readily overcome.

Assignment of aliphatic side-chain proton and carbon resonances is necessary for high resolution structure determination using NOE distance constraints. Since the assignments of C^α and C^β have been obtained by the backbone assignment, the side-chain resonance can be assigned by transferring the magnetization of backbone amide protons to side-chain spins. (H)CC(CO)NH-TOCSY (Montelione *et al.*, 1992; Grzesiek *et al.*, 1993; Logan *et al.*, 1993; Lyons and Montelione, 1993) correlates the chemical shifts of H_i^N and N_i to all C_{i-1}^{aliph} via couplings of $^1J_{NC'}$ and $^1J_{CC}$, while HCCH-TOCSY (Bax *et al.*, 1990a; Fesik *et al.*, 1990; Olejniczak *et al.*, 1992; Majumdar *et al.*, 1993) provides correlations among aliphatic protons and carbons within residues. A 3D ^{15}N HSQC-TOCSY experiment can also be used to confirm and obtain complete assignment of aliphatic ^1H resonances. For proteins larger than 30 kDa, the line widths of the aliphatic ^1H and ^{13}C resonances increase to the size comparable with the scalar couplings used for coherence transfer in the HCCH-TOCSY experiment, causing the significant reduction in sensitivity. An HCCH-NOESY experiment has been used to correlate the side-chain resonances of large proteins via NOESY in replacement of TOCSY. TROSY type experiments have successfully been used to establish backbone assignments for proteins as large as 110 kDa.

5.3. GENERAL PROCEDURE OF SETUP AND DATA PROCESSING FOR 3D EXPERIMENTS

All pulses for the transmitter and decouplers should be properly calibrated (refer to instrument calibration). The spectral windows are set on a 500 MHz spectrometer to 6,500, 1,600, 7,500 and 1,750 Hz for ^1H , ^{15}N , aliphatic ^{13}C , and $^{13}\text{C}'$, respectively, or on a 600 MHz spectrometer, 8,000, 2,000, 9,000, and 2,100 Hz for ^1H , ^{15}N , aliphatic ^{13}C , and $^{13}\text{C}'$, respectively. The carrier for ^1H is always set to H_2O resonance for aqueous samples, whereas the decoupler offset frequencies are set to the center of the chemical shift range of the indirectly observed

heteronuclear nuclei. The center of chemical shift is commonly selected as 118, 177, 54, and 40 ppm for ^{15}N , $^{13}\text{C}'$, $^{13}\text{C}^{\alpha/\beta}$, and C^{α} , respectively. The data should be collected with minimal digital resolutions for all dimensions, which typically are 0.025, 0.10, 1.00, 1.70, and 0.35 ppm/point for ^1H , ^1H indirect, ^{15}N , aliphatic ^{13}C , and $^{13}\text{C}'$, respectively. If the data are collected with an acquisition time of 64 ms, 128 complex points in the ^1H indirect dimension, 35 complex points for ^{15}N , and 40 for the ^{13}C dimension, this provides digital resolutions of 0.014, 0.10, 0.95, 1.50, and 0.35 ppm/point, respectively.

First, 1D ^1H and ^1H – ^{15}N HSQC data are collected to check the condition of the sample. Then, a 1D trail spectrum of the 3D experiment is collected with 1 scan and the t_1 and t_2 increments set to 1. The receiver gain needs to be optimized using the 1D trail spectrum. Next, two 2D slices of the 3D experiment should be collected with 16 scans and the optimized gain to make certain that the setup is correct. Other parameters include a predelay set to 1.0–1.3 s and 32 steady state scans (or dummy scans). The number of transients is set to the minimum number needed for phase cycling, usually 8 scans. If more scans are necessary, the data may be collected with fewer increments for each of the indirect dimensions.

The acquired data are converted to a specific format before they can be processed using NMRpipe (Delaglio *et al.*, 1995, 2004), NMRview (Johnson, 2004), or other software. The 2D versions of the 3D data are extracted and processed with the same procedure as in 3D processing (see following text). The spectra are phased and phase parameters are used for 3D data processing. In the observed ^1H dimension, all data are usually processed identically. Data are processed with a solvent suppression filter applied to the time domain data prior to apodization by a 70° shifted squared sine-bell function, zero filling to 1024 complex points, Fourier transform, and phasing. In the ^{13}C or indirect ^1H dimension, after size-doubling by mirror image linear prediction, the data are apodized by a 70° shifted squared sine-bell function, zero filled to 256 complex points, Fourier transformed, and phased. In the ^{15}N dimension, the data sizes are doubled by mirror image linear prediction followed by apodization with a squared cosine-bell function, zero-filling to 128 complex points, Fourier transformation, and phasing.

5.4. EXPERIMENTS FOR BACKBONE ASSIGNMENTS

Six 3D triple resonance experiments will be discussed; these were mentioned previously as being the most common experiments for making backbone assignments using uniformly ^{15}N and ^{13}C labeled proteins. Since most of the experiments include the magnetization transfer of amide protons that are exchangeable with water under normal sample conditions, water-flip-back is used in the experiments for water suppression to avoid the saturation of amide proton magnetization, which provides superior sensitivity along with the use of PEP sensitivity enhancement. In addition, the experiments utilize gradient echoes to select the desired coherence pathways in combination with limited phase cycling for PEP sensitivity enhancement and quadrature detection in the indirect dimensions. The pulse sequences discussed here are for three-channel configuration of the spectrometer, that is, RF band-specific pulses for C' and C^{α} are applied via the same RF channel of the spectrometer by applying off-resonance pulses for one of the carbon regions, which is denoted by “off” in Table 5.1. For a four-channel spectrometer, pulses for C' and C^{α} can be delivered on separate channels with the carrier set at each carbon region. In that case, on-resonance selective pulses are applied. When the magnetization of ^{15}N is selectively transferred to C' or C^{α} via INEPT, selective carbon pulses

TABLE 5.1
Parameters and Correlations of the 3D Experiments

Parameter	Experiments						
	HNCO	HNCA	HN(CO)CA	HN(CA)CO	CBCANH	CBCA(CO)NH	HCCH–TOCSY
^{13}C offset	C'	C^α	C^α	C'	$\text{C}^{\alpha,\beta}$	$\text{C}^{\alpha,\beta}$	C^{aliph}
“On” pulses	$\text{C}' 90^\circ$, 180°	$\text{C}^\alpha 90^\circ$, 180°	$\text{C}^\alpha 90^\circ$, 180°	$\text{C}' 90^\circ$, 180°	$\text{C}^{\alpha,\beta} 90^\circ$, 180°	$\text{C}^{\alpha,\beta} 90^\circ$, 180°	$\text{C}^{\text{aliph}} 90^\circ, 180^\circ$
“Off” pulses	$\text{C}^\alpha 180^\circ$	$\text{C}' 180^\circ$	$\text{C}' 90^\circ$, 180°	$\text{C}^\alpha 90^\circ$, 180°	$\text{C}' 180^\circ$	$\text{C}' 90^\circ, 180^\circ$	$\text{C}' 180^\circ$
τ (ms)	2.7	2.7	2.7	2.7	2.7	2.7	
δ (ms)	13.5	11.0	13.5	11.0			
δ_1 (ms)			7.0	3.4	1.8	1.8	1.8
δ_2 (ms)	0.5	0.5	0.5	0.5	0.5	0.5	0.8
δ_3 (ms)						4.5	1.1
τ_1 (ms)					2.0	2.4	
τ_2 (ms)					11.0	3.4	
τ_3 (ms)					11.0	13.5	
Correlations	H_i, N_i , C'_{i-1}	H_i, N_i , C^α_i , C^α_{i-1}	H_i, N_i , C^α_{i-1}	H_i, N_i , C'_i , C'_{i-1}	H_i, N_i , $\text{C}^{\alpha,\beta}_i$, $\text{C}^{\alpha,\beta}_{i-1}$	H_i, N_i , $\text{C}^{\alpha,\beta}_{i-1}$	$\text{H}^{\text{aliph}}_i$, $\text{H}^{\text{aliph}}_j$, $\text{C}^{\text{aliph}}_i$

are used to avoid exciting unwanted carbon magnetization because the scalar couplings $^1J_{\text{NC}\alpha}$ and $^1J_{\text{NC}'}$ have a similar size (11 and 15 Hz, respectively). However, non-selective carbon pulses can be applied if the magnetization transfer is from aliphatic protons to their attached carbons, because $^2J_{\text{HC}'}$ and $^3J_{\text{HC}'}$, if they are not zero, are much smaller than $^1J_{\text{HC}}$ (~ 135 Hz) and the INEPT optimized for $^1J_{\text{HC}}$ does not have magnetization transferred via $^2J_{\text{HC}'}$ and $^3J_{\text{HC}'}$.

5.4.1. HNCO and HNCA

If C^α pulses are exchanged for C' pulses, the HNCO and HNCA experiments have identical pulse sequences as shown in Figure 5.6. Of the six experiments mentioned previously, HNCO has the highest sensitivity. The HNCO spectrum contains the correlations of H_i^{N} , N_i , and C'_{i-1} but not C'_i since $^2J_{\text{N}(i)\text{C}'(i)}$ has a value close to zero, whereas HNCA gives two sets of backbone correlations, within the residue and with the preceding residue: H_i^{N} , N_i , and C^α_i as well as H_i^{N} , N_i , and C^α_{i-1} due to the fact that $^1J_{\text{NC}'}$ (11 Hz) and $^2J_{\text{NC}'}$ (15 Hz) are comparable in size.

The pulse sequences utilize the “out and back” transfer pathway to transfer the magnetization:

$$\text{HNCO: } \text{H}_\text{N} \xrightarrow{J_{\text{HN}}} \text{N} \xrightarrow{J_{\text{NC}'}} \text{C}'(t_1) \xrightarrow{J_{\text{NC}'}} \text{N}(t_2) \xrightarrow{J_{\text{HN}}} \text{H}_\text{N}(t_3) \quad (5.36)$$

$$\text{HNCA: } \text{H}_\text{N} \xrightarrow{J_{\text{HN}}} \text{N} \xrightarrow{J_{\text{NC}\alpha}} \text{C}_\alpha(t_1) \xrightarrow{J_{\text{NC}\alpha}} \text{N}(t_2) \xrightarrow{J_{\text{HN}}} \text{H}_\text{N}(t_3) \quad (5.37)$$

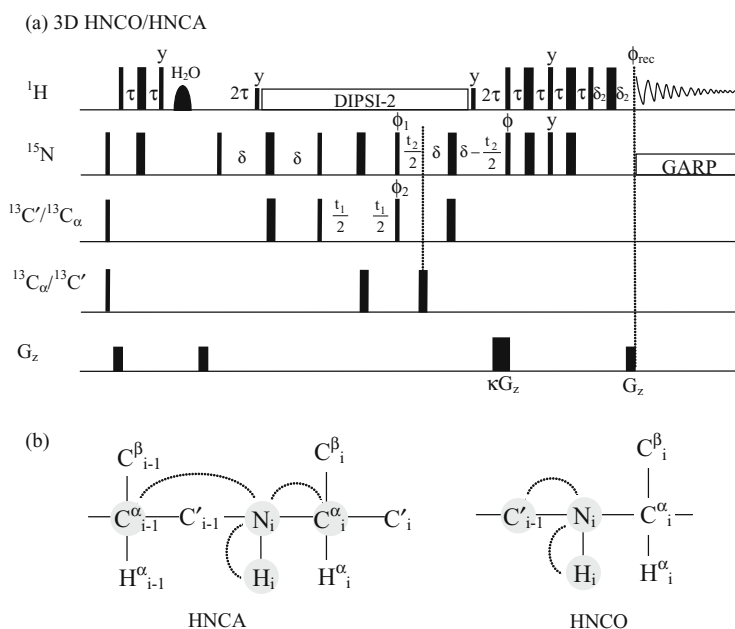


Figure 5.6. HNCO and HNCA pulse sequences (a) and the corresponding resonance connectivities (b). (a) The delay $\tau = 2.7$ ms, $\delta = 13.5$ ms for HNCO, 11.0 ms for HNCA, δ_2 equals the G_z gradient pulse length. All pulses are x phased, except that $\phi_1 = x, x, -x, -x$; $\phi_2 = x, -x, +\text{States-TPPI}$, and $\phi_{\text{rec}} = x, -x, -x, x$. For PEP, the signs of κ and ϕ are inverted: $\kappa = \pm 10$, $\phi = \pm x$. (b) The dotted lines linking shaded nuclei indicate the observed correlations for the experiments: H_i , N_i , and C^α_{i-1} and C^α_i in HNCA or H_i , N_i , and C^α_{i-1} in HNCO.

The magnetization originating from the amide proton H^N is transferred to the attached N via the $^1J_{\text{HN}}$ coupling during the INEPT sequence. The magnetization is then transferred to C' in HNCO (or C^α in HNCA) in the next INEPT during which the coupling of H^N with N is removed by DIPSI-2 proton decoupling. The delay 2δ is set to $1/(2^1J_{\text{NC}'})$, approximately 13.5 ms in HNCO [11.0 ms for HNCA, $2\delta \approx 1/(4^1J_{\text{NC}_\alpha})$] for optimizing the refocus of the coupling. After the chemical shift of carbonyl C' evolves during the t_1 evolution period, the magnetization is transferred via the “back” pathway to N and then back to its origin, H. The chemical shift evolution of N proceeds during the “back” pathway to minimize the loss in magnetization caused by relaxation during the INEPT periods involving C' , which have long delays due to the weak $^2J_{\text{NC}'}$ coupling. Spin decoupling is applied to suppress evolution under the scalar coupling interaction of J_{HN} . The other important role of ^1H decoupling is to ensure that IP coherence N_y (^{15}N spins) is generated throughout the INEPT sequences. DIPSI decoupling increases the experimental sensitivity compared to decoupling by refocusing 180° pulses because the IP coherence is not affected by T_1 relaxation in contrast to the AP coherence N_xH_z which relaxes with both T_1 and T_2 relaxation times. The two ^1H 90° pulses that are next to the DIPSI-2 sequence restore the water magnetization along $+z$ at the end of the DIPSI-2 sequence. At the beginning of pulse sequence, the 90° N and C pulses combined with the gradients after them are used to dephase all N and C magnetizations so that the observed magnetization solely originates from ^1H (contributes to the FID).

5.4.1.1. Product Operator Description of the HNCO Experiment

The magnetization transfer can be described in terms of product operators. The operators for magnetizations of ^1H , ^{15}N , and C' are denoted as H , N , and C . After the first ^1H 90° pulse generates $-\text{H}_y$ magnetization, the first INEPT sequence yields AP magnetization:

$$-\text{H}_y \xrightarrow{\tau - \pi(\text{H}_x + \text{N}_x) - \tau} -2\text{H}_x\text{N}_z \xrightarrow{\frac{\pi}{2}(\text{H}_y + \text{N}_x)} -2\text{H}_z\text{N}_y \quad (5.38)$$

in which τ is set to $1/(4J_{\text{NH}})$ so that the coefficient $\sin(2\pi J_{\text{NH}}\tau)$ of the AP magnetization has a maximum. The selective water 90° pulse brings the water magnetization to the z axis and the gradient destroys any residual transverse water magnetization.

At the end of 2τ , the ^{15}N magnetization is refocused to be an IP coherence with respect to the ^1H spin when $2\tau = 1/(2J_{\text{NH}})$, which leads to $\sin(\pi J_{\text{NH}}2\tau) = 1$ and $\cos(\pi J_{\text{NH}}2\tau) = 0$:

$$-2\text{H}_z\text{N}_y \xrightarrow{2\tau} \text{N}_x \quad (5.39)$$

A ^1H 90° pulse before the DIPSI-2 sequence brings water magnetization back to the transverse plane, which is then brought back to the z axis by the 90° ^1H pulse at the end of DIPSI-2. The N magnetization transfers to C' via the next INEPT:

$$\text{H}_x \xrightarrow{\delta \rightarrow \pi(\text{N}_x + \text{C}_x) \rightarrow \delta} 2\text{N}_y\text{C}_z \xrightarrow{\frac{\pi}{2}(\text{N}_x + \text{C}_x)} -2\text{N}_z\text{C}_y \quad (5.40)$$

The delay δ is set to $1/(4J_{\text{NC}'})$, causing $\sin(2\pi J_{\text{NC}'}\delta) = 1$. During t_1 evolution both N and C^α spins are decoupled from C' by the refocusing 180° pulses in the middle of t_1 . After the C' chemical shift evolves, the magnetization is transferred from C' back to N by the two 90° pulses:

$$-2\text{N}_z\text{C}_y \xrightarrow{t_1} 2\text{N}_z\text{C}_y \cos(\Omega_{\text{C}'}t_1) \xrightarrow{\frac{\pi}{2}(\text{N}_x + \text{C}_x)} -2\text{N}_y\text{C}_z \cos(\Omega_{\text{C}'}t_1) \quad (5.41)$$

The sine-modulated multiple-quantum component generated during t_1 will not contribute to the observable magnetization and hence is omitted from consideration. During the constant time t_2 evolution period, ^1H is still being decoupled by DIPSI-2 decoupling and C^α is decoupled by the $\text{C}'180^\circ$ refocus pulse during the initial period of t_2 and by $\text{C}^\alpha 180^\circ$ and $\text{N} 180^\circ$ in the remaining t_2 period. The NC' coupling evolves for the entire 2δ that is set to $\delta = 1/(4J_{\text{NC}'})$ to have $\sin(2\pi J_{\text{NC}'}\delta) = 1$, whereas an N chemical shift evolves for the period of t_2 , resulting in:

$$-2\text{N}_y\text{C}_z \cos(\Omega_{\text{C}'}t_1) \xrightarrow{2\delta} \text{N}_x \cos(\Omega_{\text{C}'}t_1) \quad (5.42)$$

$$\text{N}_x \cos(\Omega_{\text{C}'}t_1) \xrightarrow{t_2} \text{N}_x \cos(\Omega_{\text{C}'}t_1) \cos(\Omega_{\text{N}}t_2) + \text{N}_y \cos(\Omega_{\text{C}'}t_1) \sin(\Omega_{\text{N}}t_2) \quad (5.43)$$

The N magnetization evolves during the 2τ period after DIPSI-2 under the influence of $^1J_{\text{NH}}$ coupling, resulting in two AP coherences:

$$\begin{aligned} &\text{N}_x \cos(\Omega_{\text{C}'}t_1) \cos(\Omega_{\text{N}}t_2) + \text{N}_y \cos(\Omega_{\text{C}'}t_1) \sin(\Omega_{\text{N}}t_2) \xrightarrow{2\tau} \\ &2\text{H}_z\text{N}_y \cos(\Omega_{\text{C}'}t_1) \cos(\Omega_{\text{N}}t_2) - 2\text{H}_z\text{N}_x \cos(\Omega_{\text{C}'}t_1) \sin(\Omega_{\text{N}}t_2) \end{aligned} \quad (5.44)$$

The last period in the pulse sequence is for the PEP sensitivity enhancement sequence in which the two terms of the coherence can be considered separately. The first FID is acquired with $\phi = y$ and $\kappa = 10$ and the second one is recorded with both the phase ϕ and gradient κ inverted. To simplify, the coefficients are temporarily dropped and will be retrieved later, since they are not changed by the PEP sequence. During the PEP, the evolution from the first term yields:

$$2H_zN_y \xrightarrow{\frac{\pi}{2}(H_x+N_x)} -2H_yN_z \quad (5.45)$$

$$-2H_yN_z \xrightarrow{\tau \rightarrow \pi(H_x+N_x) \rightarrow \tau} H_x \xrightarrow{\frac{\pi}{2}(H_y+N_y)} -H_z \quad (5.46)$$

$$-H_z \xrightarrow{\tau \rightarrow \pi(H_x+N_x) \rightarrow \tau} H_z \xrightarrow{\frac{\pi}{2}H_x} -H_y \quad (5.47)$$

The second term evolves:

$$-2H_zN_x \xrightarrow{\frac{\pi}{2}(H_x+N_x)} 2H_yN_x \quad (5.48)$$

Because H_yN_x is multiple-quantum coherence, it does not evolve under the influence of scalar coupling.

$$2H_yN_x \xrightarrow{\tau \rightarrow \pi(H_x+N_x) \rightarrow \tau} 2H_yN_x \xrightarrow{\frac{\pi}{2}(H_y+N_y)} -2H_yN_z \quad (5.49)$$

$$-2H_yN_z \xrightarrow{\tau \rightarrow \pi(H_x+N_x) \rightarrow \tau \rightarrow \frac{\pi}{2}H_x} H_x \quad (5.50)$$

After retrieving the coefficients for both terms, the observable magnetization has a form of:

$$H_x \cos(\Omega_C t_1) \sin(\Omega_N t_2) - H_y \cos(\Omega_C t_1) \cos(\Omega_N t_2) \quad (5.51)$$

The last ^1H 180° pulse is used to invert ^1H magnetization for coherence selection by the gradient. The delay δ_1 is set to be long enough for the gradient plus gradient recovery time.

The second data set is recorded with inverted ϕ and gradient factor κ . For the first term:

$$2H_zN_y \xrightarrow{\frac{\pi}{2}(H_x-N_x)} 2H_yN_z \quad (5.52)$$

$$2H_yN_z \xrightarrow{\tau \rightarrow \pi(H_x+N_x) \rightarrow \tau} -H_x \xrightarrow{\frac{\pi}{2}(H_y+N_y)} H_z$$

$$\xrightarrow{\tau \rightarrow \pi(H_x+N_x) \rightarrow \tau} -H_z \xrightarrow{\frac{\pi}{2}H_x} H_y \quad (5.53)$$

For the second term,

$$-2H_zN_x \xrightarrow{\frac{\pi}{2}(H_x-N_x)} 2H_yN_x \quad (5.54)$$

which is the same as in the first FID. Therefore, this term remains the same:

$$2H_yN_x \xrightarrow{\tau \rightarrow \pi(H_x+N_x) \rightarrow \tau} 2H_yN_x \xrightarrow{\frac{\pi}{2}(H_y+N_y)} -2H_yN_z \xrightarrow{\tau \rightarrow \pi(H_x+N_x) \rightarrow \tau \rightarrow \frac{\pi}{2}H_x} H_x \quad (5.55)$$

The second FID has a form of:

$$H_x \cos(\Omega_C t_1) \sin(\Omega_N t_2) + H_y \cos(\Omega_C t_1) \cos(\Omega_N t_2) \quad (5.56)$$

The two obtained FIDs are:

$$\begin{cases} H_x \cos(\Omega_C t_1) \sin(\Omega_N t_2) - H_y \cos(\Omega_C t_1) \cos(\Omega_N t_2) \\ H_x \cos(\Omega_C t_1) \sin(\Omega_N t_2) + H_y \cos(\Omega_C t_1) \cos(\Omega_N t_2) \end{cases} \quad (5.57)$$

Addition of the two FIDs gives rise to a PEP data set which contains the observable magnetization described by:

$$2H_x \cos(\Omega_C t_1) \sin(\Omega_N t_2) \quad (5.58)$$

Similarly, subtraction of the two FIDs ($FID_2 - FID_1$) yields another PEP data set:

$$2H_y \cos(\Omega_C t_1) \cos(\Omega_N t_2) \quad (5.59)$$

The two PEP data sets can be processed to obtain separate 3D spectra. The two spectra are then combined to form a single spectrum with pure absorptive line shapes in all three dimensions. Alternatively, the data sets can be combined before Fourier transformation.

5.4.1.2. *HNCO Experiment Setup*

The transmitter channel is set to the ^1H frequency with the carrier frequency on the water resonance. The first decoupler channel is used for ^{13}C with the offset frequency set to the middle of carbonyl C' (177 ppm) whereas the ^{15}N pulses are applied on the second decoupler channel with the offset frequency in the middle of the ^{15}N spectral window (118 ppm). The pulse calibration for ^1H includes a 90° hard pulse, a 90° pulse for broadband decoupling (WALTZ16 or DIPSI-2; $\sim 100 \mu\text{s}$), and a water selective 90° pulse (see section on instrument calibration). Pulses for ^{13}C and ^{15}N are not required to be calibrated for every experiment setup, meaning that the pulse lengths can be used repeatedly after they are calibrated periodically. The hard 90° ^{15}N pulse is normally shorter than $40 \mu\text{s}$ and the 90° pulse length for GARP decoupling is about $250 \mu\text{s}$. The ^{13}C pulses used in HNCO are C' 90° pulse nulling at C^α ($64.7 \mu\text{s}$ for 500 MHz and $53.9 \mu\text{s}$ for 600 MHz), C' 180° pulse nulling at C^α ($57.9 \mu\text{s}$ for 500 MHz and $48.3 \mu\text{s}$ for 600 MHz), and a shaped C^α 180° off-resonance pulse. Alternatively, the rectangular on-resonance C' pulses can also be replaced by selective pulses such as eBURP (Geen and Freeman, 1991), or G_4 (90° excitation), and G_3 (180° inversion) with a bandwidth of 50–60 ppm (Emsley and Bodenhausen, 1990). The C^α 180° off-resonance pulses for decoupling are applied by SEDUCE shaped pulses (Coy and Mueller, 1993; see Table 4.1).

The delay 2τ is optimized to 5.4 ms, which is used to cancel the coefficient $\sin(2\pi * ^1J_{\text{NH}} * 2\tau)$ with a $^1J_{\text{NH}}$ of 90 Hz while delay δ is optimized to 13.5 ms, according to 2δ which is approximately $1/(2^1J_{\text{NC}'})$ with $^1J_{\text{NC}'}$ of 15 Hz for effective refocusing of $^1J_{\text{NC}'}$. These delays are optimized by recording a 1D experiment to obtain the most intense signals. The gradient echo pulses used for coherence selection are set to 2 ms and $200 \mu\text{s}$ with the strength of approximately 20 G cm^{-1} for the dephasing and refocusing gradient pulses, respectively. The length of the refocus gradient should be optimized to obtain the best sensitivity. For dephasing water, the gradient is applied with a strength of approximately 15 G cm^{-1} for a duration of 2 ms.

Before acquisition can be started for 3D data collection, 2D $^1\text{H}/^{15}\text{N}$ and $^1\text{H}/^{13}\text{C}$ slices of the experiments are recorded first to make sure that the number of transients is sufficient, and all parameters are optimized to yield reasonable sensitivity. To collect a $^1\text{H}/^{15}\text{N}$ 2D slice, the t_1 increment is set to 1 and the t_2 increment to 50 while the $^1\text{H}/^{13}\text{C}$ 2D slice is collected with 100 t_1 increments and a single t_2 increment. Once the 2D spectra indicate the experiment works correctly, the 3D experiment is recorded with 35 complex points for ^{15}N and 40 for ^{13}C . HNCO data are processed using the procedure described in “General Procedure for Processing 3D Data.”

5.4.1.3. HNCA

After interchanging C' and C^α pulses, the basic setup of HNCA is identical to HNCO with a few changes. The off-resonance C' 180° pulse is generated with an offset of positive 122 ppm (downfield from the carrier). The delay δ is optimized to 11 ms using $2\delta = 1/(4^1J_{\text{NC}\alpha})$, according to the coefficients for intra- and inter-residue coherence transfers:

$$\begin{aligned}\Gamma(^1J_{\text{NC}\alpha}) &= \sin(2\pi^1J_{\text{NC}\alpha}\delta) \cos(2\pi^2J_{\text{NC}\alpha}\delta) \\ \Gamma(^2J_{\text{NC}\alpha}) &= \sin(2\pi^2J_{\text{NC}\alpha}\delta) \cos(2\pi^1J_{\text{NC}\alpha}\delta)\end{aligned}\quad (5.60)$$

In addition, HNCA may require more transients to obtain a good S/N ratio because it is at least 50% less sensitive than HNCO. Since $^1J_{\text{NC}\alpha}$ (11 Hz) and $^2J_{\text{NC}\alpha}$ (7 Hz) have a similar size, correlations of H_i, N_i to both the intra-residue C_i^α and the C_{i-1}^α of the preceding residue are observed in the experiment.

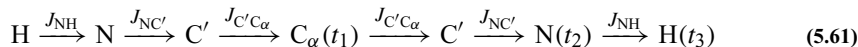
In summary, ^1H magnetization is the starting magnetization that is transferred to ^{15}N by INEPT in both sequences. The first period 2τ lets the AP magnetization evolve to IP magnetization, which is further transferred to ^{13}C by the second INEPT. This period is an important step because it allows coherence after evolving in the real time (RT) t_1 period to be transferred back to ^{15}N by a pair of 90° $^{15}\text{N}/^{13}\text{C}$ pulses, which requires fewer 180° pulses in the sequences. In the last step of the coherence transfer pathway, the ^{15}N coherence is transferred back to protons by the reversed INEPT after evolving in the constant time (CT) t_2 period. It has been noted that the RT ^{13}C and CT ^{15}N evolutions provide optimal sensitivity compared to other combinations. The other 2τ period after DIPSI-2 converts the two IP coherences into AP, which are ready to be manipulated by the PEP enhancement method. This delay–DIPSI–delay combination appears frequently in multidimensional NMR spectroscopy and will be met again in following pulse sequences.

5.4.2. HN(CO)CA

HN(CO)CA correlates amide ^1H and ^{15}N chemical shifts (H_i and N_i) with the ^{13}C chemical shift of the preceding residue, C_{i-1}^α , which is used to establish the backbone sequential connectivity across the peptide bond. By combining the information provided here with that from HNCA, both intra- and inter-residue connectivities can be distinguished. Since the stronger one-bond spin couplings ($^1J_{\text{NC}'}$ and $^1J_{\text{C}'\text{C}_\alpha}$) are utilized in HN(CO)CA compared to couplings ($^1J_{\text{NC}_\alpha}$ and $^2J_{\text{NC}_\alpha}$) used in HNCA, the magnetization transfer is more efficient. Therefore, HN(CO)CA is more sensitive than HNCA.

The HN(CO)CA pulse sequence shown in Figure 5.7 is derived from HNCO by transferring the magnetization from N to C' and then from C' to C^α via $^1J_{\text{NC}'}$ and $^1J_{\text{C}'\text{C}_\alpha}$, respectively.

The pulse sequence uses an “out and back” transfer pathway:



After the ^1H magnetization is transferred to N during INEPT, the N magnetization is transferred to carbonyl C' via the second INEPT sequence. The transfer of C' magnetization to C $^\alpha$ is achieved by an HMQC-type sequence, which has been demonstrated to be superior for the $J_{\text{C}'\text{C}^\alpha}$ magnetization transfer. After a C $^\alpha$ chemical shift evolves during t_1 , the magnetization is transferred back through the reverse pathway. The evolution of an N chemical shift takes place during t_2 along the reverse pathway, before the coherence is transferred to H for detection. A PEP building block sequence combined with gradients is used to achieve sensitivity enhancement. The ^1H selective pulse on water is to align the water magnetization along the z axis.

The magnetization transfer in the pulse sequence can be described by product operators, which are denoted as H, N, C', and C $^\alpha$ for amide ^1H , ^{15}N , carbonyl ^{13}C , and $^{13}\text{C}^\alpha$. The

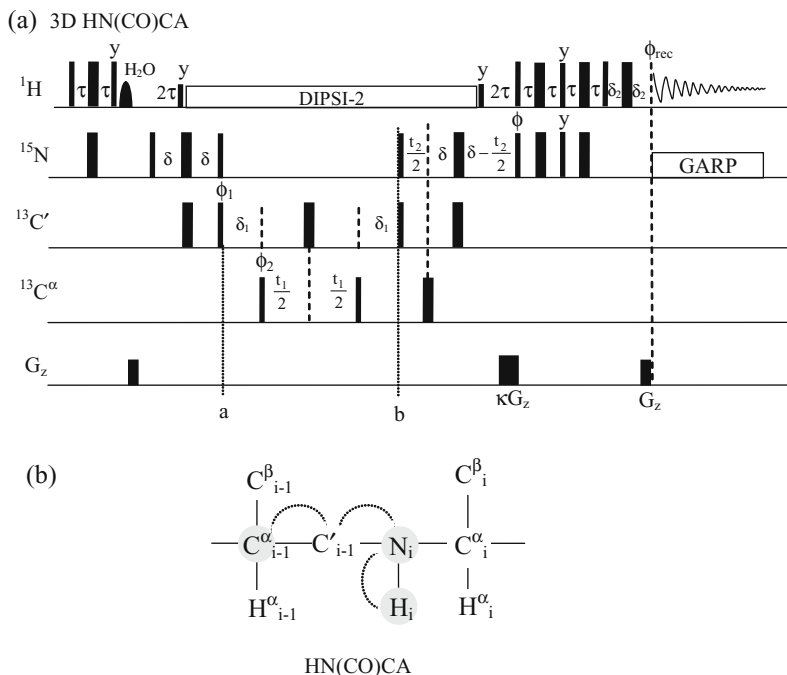


Figure 5.7. Pulse sequence of 3D HN(CO)CA. The experiment is derived from HNCO. An HMQC-type sequence is used to transfer the magnetization from C' to C $^\alpha$ and then back to C'. The phase cycles of ϕ_1 and ϕ_2 are the same as in HNCO. For PEP, the signs of κ and ϕ are inverted: $\kappa = \pm 10$, $\phi = \pm x$. The delays are set to $\tau = 2.7$ ms, $\delta = 13.5$ ms, $\delta_1 = 7.0$ ms, and δ_2 equals the G_z gradient length. The ^{13}C offset frequency is set on C $^\alpha$ as in the HNCO experiment. Pulses on C $^\alpha$ are selective pulses which do not excite C', while C' pulses are off-resonance selective pulses (shaped pulses; see Table 4.1). (b) The dotted lines indicate the magnetization transfer and the observed correlations are between the shaded H_i , N_i , and C_{i-1}^α relayed via C_{i-1}' .

coherence transfer from ^1H to ^{15}N and then to $^{13}\text{C}'$ is the same as that in an HNCO experiment [Equations (5.38) to (5.40)]:

$$\begin{aligned} \text{H}_z & \xrightarrow{\frac{\pi}{2} \text{H}_x \rightarrow \tau \rightarrow \pi(\text{H}_x) \rightarrow \tau \rightarrow \frac{\pi}{2}(\text{H}_y + \text{N}_x) \rightarrow 2\tau} \text{N}_x \\ & \xrightarrow{\delta \rightarrow \pi(\text{N}_x + \text{C}'_x) \rightarrow \delta \rightarrow \frac{\pi}{2}(\text{N}_x + \text{C}'_x)} -2\text{N}_z \text{C}'_y \end{aligned} \quad (5.62)$$

in which $\tau = 1/(4J_{\text{HN}})$ and $\delta = 1/(4J_{\text{NC}'})$. The magnetization is then transferred to C^α and then back to C' after t_1 evolution during an HMQC-type sequence:

$$\begin{aligned} -2\text{N}_z \text{C}'_y & \xrightarrow{\delta_1 \rightarrow \frac{\pi}{2} \text{C}'_x} -4\text{N}_z \text{C}'_x \text{C}'_y \\ & \xrightarrow{\frac{t_1}{2} \rightarrow \pi \text{C}'_x \rightarrow \frac{t_1}{2} \rightarrow \frac{\pi}{2} \text{C}'_x \rightarrow \delta_1} -2\text{N}_z \text{C}'_y \cos(\Omega_{\text{C}} t_1) \end{aligned} \quad (5.63)$$

in which $\delta_1 = 1/(2J_{\text{C}'\text{C}_\alpha})$. In practice, the delay δ_1 is set to a value in between $1/(3J_{\text{C}'\text{C}_\alpha})$ and $1/(2J_{\text{C}'\text{C}_\alpha})$, 7.0 ms. The magnetization transfer in the reverse INEPT sequence and sensitivity-enhancement PEP sequence in HN(CO)CA, which are identical to those in HNCO, yield two FIDs:

$$\begin{aligned} & -2\text{N}_z \text{C}'_y \cos(\Omega_{\text{C}} t_1) \xrightarrow{\frac{\pi}{2}(\text{N}_x + \text{C}_x)} 2\text{N}_y \text{C}'_z \cos(\Omega_{\text{C}} t_1) \\ & \xrightarrow{2\delta} -\text{N}_x \cos(\Omega_{\text{C}} t_1) \\ & \xrightarrow{t_2} -\text{N}_x \cos(\Omega_{\text{C}} t_1) \cos(\Omega_{\text{N}} t_2) - \text{N}_y \cos(\Omega_{\text{C}} t_1) \sin(\Omega_{\text{N}} t_2) \\ & \xrightarrow{2\tau} -2\text{H}_z \text{N}_y \cos(\Omega_{\text{C}} t_1) \cos(\Omega_{\text{N}} t_2) + 2\text{H}_z \text{N}_x \cos(\Omega_{\text{C}} t_1) \sin(\Omega_{\text{N}} t_2) \end{aligned} \quad (5.64)$$

in which τ and δ are the same as in equation (5.62). The first FID after PEP is given by:

$$\text{H}_x \cos(\Omega_{\text{C}} t_1) \sin(\Omega_{\text{N}} t_2) - \text{H}_y \cos(\Omega_{\text{C}} t_1) \cos(\Omega_{\text{N}} t_2) \quad (5.65)$$

and the second FID is proportional to:

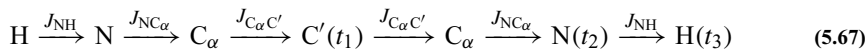
$$\text{H}_x \cos(\Omega_{\text{C}} t_1) \sin(\Omega_{\text{N}} t_2) + \text{H}_y \cos(\Omega_{\text{C}} t_1) \cos(\Omega_{\text{N}} t_2) \quad (5.66)$$

The two FIDs are acquired separately and stored in different memory locations. The addition and subtraction of the two FIDs yield two data sets that can be processed separately and combined to a single spectrum with absorptive phase.

5.4.3. HN(CA)CO

The HN(CA)CO experiment provides correlations of H_i^{N} , N_i , and C'_i chemical shifts. Similar to HNCA, the sequential connectivities from H_i^{N} , N_i to C'_{i-1} are also observed in the experiment owing to the comparable size of the scalar couplings $^1J_{\text{NC}\alpha}$ and $^2J_{\text{NC}\alpha}$. Because of the low sensitivity caused by the weak couplings, a fraction of the correlations may not be observed in the experiment.

A sensitivity enhanced version of the HN(CA)CO experiment shown in Figure 5.8 is derived from the HNCA experiment. The pulse sequence uses the “out and back” transfer pathway:



After the magnetization originating from amide protons is transferred to the N spins via the INEPT sequence, the amide ^{15}N magnetization is transferred to $\text{C}\alpha$ via the next INEPT sequence. The $\text{C}\alpha$ magnetization is further transferred to C' , followed by the evolution of C' chemical shifts. During the reverse transfer path, the coherence is transferred back via $\text{C}\alpha$ and amide ^{15}N spins to amide protons for detection. The amide ^{15}N chemical shifts evolve during the constant-time evolution t_2 . The product operator terms leading to observable magnetization throughout the transfers at the indicated time points in the pulse sequence are

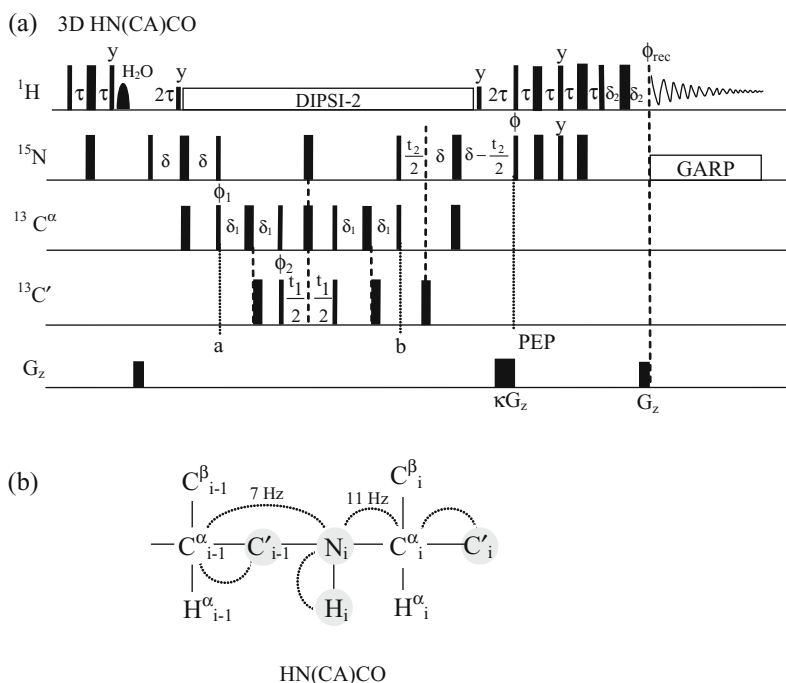


Figure 5.8. Pulse sequence of HN(CA)CO. The experiment is derived for HNCA. An INEPT sequence is used for all steps of the out-back transfer. All phases are the same as in the HN(CO)CA sequence. Delays are set to $\delta_1 = 3.4$ ms and $\delta = 11$ ms. The ^{13}C offset frequency is set on C' as in HNCA. Pulses on C' are selective pulses that do not excite $\text{C}\alpha$, while $\text{C}\alpha$ pulses are off-resonance selective pulses (shaped pulses; see Table 4.1). (b) The dotted lines indicate the magnetization transfer pathways and the observed correlations are indicated by the shaded nuclei: H_i , N_i , C'_{i-1} , and C'_i relayed via C^{α}_{i-1} and C^{α}_i .

given by:

$$\begin{aligned} \text{H}_z &\xrightarrow{\frac{\pi}{2} \text{H}_x \rightarrow \tau \rightarrow \pi(\text{H}_x + \text{N}_x) \rightarrow \tau \rightarrow \frac{\pi}{2}(\text{H}_y + \text{N}_x) \rightarrow 2\tau} \text{N}_x \\ &\xrightarrow{\delta \rightarrow \pi(\text{N}_x + \text{C}_x^\alpha) \rightarrow \delta \rightarrow \frac{\pi}{2}(\text{N}_x + \text{C}_x^\alpha)} -2\text{N}_z \text{C}_y^\alpha \end{aligned} \quad (5.68)$$

in which $\tau = 1/(4J_{\text{HN}})$, and $\delta = 1/(8J_{\text{NC}\alpha})$ to optimize for both intra- and inter-residue coherence transfer [equation (5.60)]. At point *a*:

$$\begin{aligned} -2\text{N}_z \text{C}_y^\alpha &\xrightarrow{\delta_1 \rightarrow \pi(\text{C}_x^\alpha + \text{C}_x') \rightarrow \delta_1 \rightarrow \frac{\pi}{2}(\text{C}_x^\alpha + \text{C}_x')} -4\text{N}_z \text{C}_x^\alpha \text{C}_y' \\ &\xrightarrow{\frac{t_1}{2} \rightarrow \pi(\text{C}_x^\alpha + \text{N}_x) \rightarrow \frac{t_1}{2} \rightarrow \frac{\pi}{2}(\text{C}_x^\alpha + \text{C}_x')} -4\text{N}_z \text{C}_x^\alpha \text{C}_z' \cos(\Omega_{\text{C}'} t_1) \\ &\xrightarrow{\delta_1 \rightarrow \pi(\text{C}_x^\alpha + \text{C}_x') \rightarrow \delta_1 \rightarrow \frac{\pi}{2}(\text{N}_x' + \text{C}_x')} 2\text{N}_y \text{C}_z^\alpha \cos(\Omega_{\text{C}'} t_1) \end{aligned} \quad (5.69)$$

in which $\delta_1 = 1/(4J_{\text{C}'\text{C}\alpha})$ and is optimized to a value between $1/(4J_{\text{C}'\text{C}\alpha})$ and $1/(6J_{\text{C}'\text{C}\alpha})$, 3.4 ms. At point *b*:

$$\begin{aligned} 2\text{N}_y \text{C}_z^\alpha \cos(\Omega_{\text{C}'} t_1) &\xrightarrow{2\delta} -\text{N}_x \cos(\Omega_{\text{C}'} t_1) \\ &\xrightarrow{t_2} -\text{N}_x \cos(\Omega_{\text{C}'} t_1) \cos(\Omega_{\text{N}} t_2) - \text{N}_y \cos(\Omega_{\text{C}'} t_1) \sin(\Omega_{\text{N}} t_2) \\ &\xrightarrow{2\tau} -2\text{H}_z \text{N}_y \cos(\Omega_{\text{C}'} t_1) \cos(\Omega_{\text{N}} t_2) + 2\text{H}_z \text{N}_x \cos(\Omega_{\text{C}'} t_1) \sin(\Omega_{\text{N}} t_2) \end{aligned} \quad (5.70)$$

in which τ and δ are set as in equation (5.68). The PEP sequence yields two FIDs:

$$\begin{aligned} &\text{H}_x \cos(\Omega_{\text{C}'} t_1) \sin(\Omega_{\text{N}} t_2) - \text{H}_y \cos(\Omega_{\text{C}'} t_1) \cos(\Omega_{\text{N}} t_2) \\ &\text{H}_x \cos(\Omega_{\text{C}'} t_1) \sin(\Omega_{\text{N}} t_2) + \text{H}_y \cos(\Omega_{\text{C}'} t_1) \cos(\Omega_{\text{N}} t_2) \end{aligned} \quad (5.71)$$

which are stored in different memory locations and are treated as described above.

5.4.4. CBCANH

The 3D CBCANH experiment correlates resonances of H_i^{N} and N_i with C_i^α and C_i^β , and C_{i-1}^α and C_{i-1}^β carbons. The correlation to residue $i - 1$ is caused by the similar values of the couplings of C_{i-1}^α and C_i^α to N_i . For each amide H or N resonance, there are four cross-peaks in the spectrum, which provides information about the amino acid type of residues and reduces the effect of $\text{C}^\alpha\text{--H}$ degeneracy for assignment. The experiment allows not only complete sequential assignments but also assignment of side-chain carbons, which is useful information for complete assignment of aliphatic resonances using the 3D HCCH–TOCSY experiment. The experiment is a transfer type, which makes use of a relayed-COSY sequence to transfer C^β to C^α before the coherence is transferred to amide N

spins:

$$H_{\alpha,\beta} \xrightarrow{J_{C_{\alpha\beta}H}} C_{\alpha,\beta}(t_1) \xrightarrow{J_{C_{\alpha}C_{\beta}}} C_{\alpha} \xrightarrow{J_{C_{\alpha}N}} N(t_2) \xrightarrow{J_{NH}} H(t_3) \quad (5.72)$$

The product operators representing the observable coherence throughout the transfers in the pulse sequence (Figure 5.9) are given by:

$$H_z \xrightarrow{\frac{\pi}{2}H_x \rightarrow \delta_1 \rightarrow \pi(H_x + C_x^{\alpha,\beta}) \rightarrow \delta_1 \rightarrow \frac{\pi}{2}(H_y + C_x^{\alpha,\beta})} -2H_z C_y^{\alpha,\beta} \quad (5.73)$$

in which $C_y^{\alpha,\beta} = C_y^{\alpha} + C_y^{\beta}$. Because of the 1H decoupling the CH coupling evolves for only t_1 period during the constant time evolution period:

$$-2H_z C_y^{\alpha,\beta} \xrightarrow{\pi J_{C_{\alpha\beta}H} \tau_1} -2H_z C_y^{\alpha,\beta} \cos(\pi J_{C_{\alpha\beta}H} \tau_1) + C_x^{\alpha,\beta} \sin(\pi J_{C_{\alpha\beta}H} \tau_1) \quad (5.74)$$

The delay δ_1 is set to 1.8 ms and is optimized for $J_{C_{\alpha\beta}H}$ couplings, $1/(4J_{C_{\alpha\beta}H})$ and τ_1 is set to 2.2 ms to simultaneously optimize the CH_n coherence transfers of methine, methylene, and methyl groups (Figure 5.10). The gradient pulse after the 90° 1H pulse dephases all transverse magnetization. The $C_{\alpha}-C_{\beta}$ coupling evolves as follows:

$$C_x^{\alpha,\beta} \xrightarrow{t_1} (C_x^{\alpha} + C_x^{\beta}) \cos(\Omega_{C_{\alpha,\beta}} t_1) \quad (5.75)$$

$$(C_x^{\alpha} + C_x^{\beta}) \cos(\Omega_{C_{\alpha,\beta}} t_1) \xrightarrow{2T_1} \left[C_x^{\alpha} \cos(2\pi J_{C_{\alpha}C_{\beta}} T_1) + 2C_y^{\alpha} C_z^{\beta} \sin(2\pi J_{C_{\alpha}C_{\beta}} T_1) \right. \\ \left. + C_x^{\beta} \cos(2\pi J_{C_{\alpha}C_{\beta}} T_1) + 2C_z^{\alpha} C_y^{\beta} \sin(2\pi J_{C_{\alpha}C_{\beta}} T_1) \right] \cos(\Omega_{C_{\alpha,\beta}} t_1) \quad (5.76)$$

The time constant T_1 is set to $T_1 = 1/(8J_{C_{\alpha}C_{\beta}}) = 3.6$ ms and only C^{α} magnetization terms, C_x^{α} and $2C_z^{\alpha} C_y^{\beta}$, will be transferred to N in the following steps.

$$\left(C_x^{\alpha} + 2C_z^{\alpha} C_y^{\beta} \right) \cos(\Omega_{C_{\alpha,\beta}} t_1) \xrightarrow{\frac{\pi}{2} C_x^{\alpha,\beta}} \left(C_x^{\alpha} - 2C_y^{\alpha} C_z^{\beta} \right) \cos(\Omega_{C_{\alpha,\beta}} t_1) \\ \xrightarrow{2\pi J_{C_{\alpha}C_{\beta}} \tau_2} C_x^{\alpha} \cos(\Omega_{C_{\alpha,\beta}} t_1) [\cos(2\pi J_{C_{\alpha}C_{\beta}} \tau_2) + \sin(2\pi J_{C_{\alpha}C_{\beta}} \tau_2)] \quad (5.77)$$

$J_{C_{\alpha}C_{\beta}}$ coupling evolves for $2\tau_2$ period. The first term $[\cos(2\pi J_{C_{\alpha}C_{\beta}} \tau_2)]$ is from C^{α} and the second term $[\sin(2\pi J_{C_{\alpha}C_{\beta}} \tau_2)]$ is from C^{β} . Then, the coherence is transferred to N via $^1J_{C_{\alpha,\beta}N}$ and $^2J_{C_{\alpha,\beta}N}$ during the INEPT sequence:

$$\xrightarrow{\tau_2 \rightarrow \pi(C_x^{\alpha,\beta} + N_x) \rightarrow \tau_2} 2C_y^{\alpha} N_z \cos(\Omega_{C_{\alpha,\beta}} t_1) [\sin(2\pi ^1J_{C_{\alpha}N} \tau_2) \cos(2\pi ^2J_{C_{\alpha}N} \tau_2) \cos(2\pi J_{C_{\alpha}C_{\beta}} \tau_2) \\ + \sin(2\pi ^1J_{C_{\alpha}N} \tau_2) \cos(2\pi ^2J_{C_{\alpha}N} \tau_2) \sin(2\pi J_{C_{\alpha}C_{\beta}} \tau_2) \\ + \sin(2\pi ^2J_{C_{\alpha}N} \tau_2) \cos(2\pi ^1J_{C_{\alpha}N} \tau_2) \cos(2\pi J_{C_{\alpha}C_{\beta}} \tau_2) \\ + \sin(2\pi ^2J_{C_{\alpha}N} \tau_2) \cos(2\pi ^1J_{C_{\alpha}N} \tau_2) \sin(2\pi J_{C_{\alpha}C_{\beta}} \tau_2)] \quad (5.78)$$

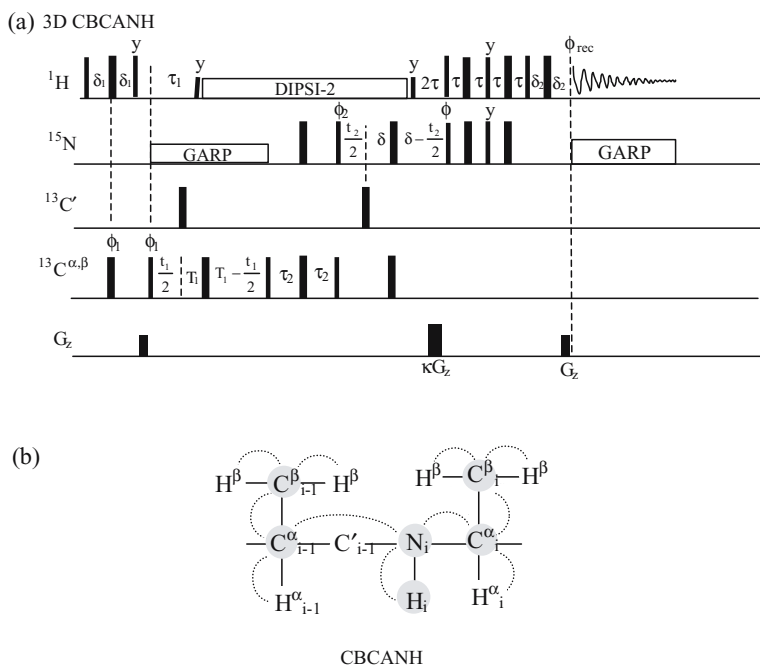


Figure 5.9. Pulse sequence of 3D CBCANH. The magnetization starts from the H^α and H^β protons and is finally transferred to HN protons and an INEPT sequence is used for all steps of the out-back transfer. The phase cycles of ϕ_1 and ϕ_2 are the same as in HNCO (Figure 5.2). The delays are set to $\delta_1 = 1.8$ ms, $\tau_1 = 2.2$ ms, $T_1 = 3.6$ ms, $\tau_2 = 11$ ms, $\delta = 11$ ms, $\tau = 2.7$ ms, and δ_2 equals the G_z gradient pulse length. (b) The dotted lines indicate the magnetization transfer pathways and the observed correlations are indicated by the shaded nuclei: H_i , N_i , C_{i-1}^α , C_{i-1}^β , C_i^α , and C_i^β .

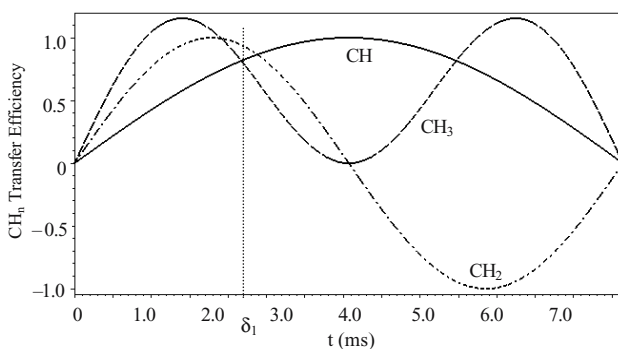


Figure 5.10. Coherence transfer efficiency via INEPT for different CH_n groups with a J_{CH} coupling constant of 140 Hz. The delay τ_1 in the CBCANH experiment is set to 2.2 ms (indicated by the dotted vertical line) to simultaneously optimize the CH_n coherence transfers of methine, methylene, and methyl groups.

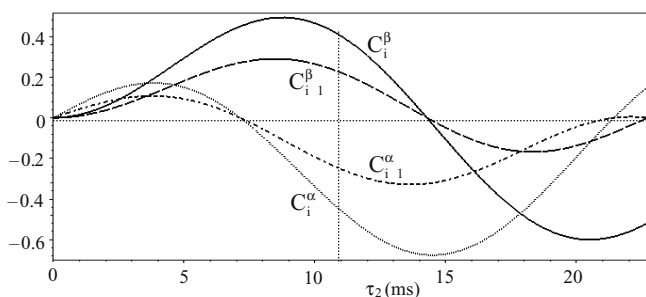


Figure 5.11. Transfer amplitude as a function of τ_2 in the CBCANH experiment using equation (5.78). The dotted vertical line at 11 ms indicates the value of τ_2 optimized for all four coherence transfer pathways using $^1J_{C_\alpha C_\beta} = 35$ Hz, $^1J_{C_\alpha N} = 11$ Hz and $^2J_{C_\alpha N} = 7$ Hz. The opposite sign of the C^α transfer amplitudes to the C^β indicates that C^α cross-peaks of the CBCANH spectrum have opposite sign relative to the C^β cross-peaks, except glycine.

in which the first two terms correspond to the coherence transfers of C_i^α and C_i^β , while the last two terms are for those of C_{i-1}^α and C_{i-1}^β , respectively. The delay τ_2 is optimized to 11 ms (Figure 5.11) according to the above coefficients. During the next constant time evolution period, the coherence evolves for $\delta - (\tau - \delta) + \tau = 2\delta$ under the influence of $J_{C_\alpha N}$, while the evolution caused by J_{NH} lasts for a period of 2τ :

$$\begin{aligned}
 2C_y^\alpha N_z \cos(\Omega_{C_{\alpha,\beta}} t_1) &\xrightarrow{\frac{\pi}{2}(C_x^\alpha + N_x)} -2N_y C_z^\alpha \cos(\Omega_{C_{\alpha,\beta}} t_1) \\
 &\xrightarrow{2\delta} N_x \cos(\Omega_{C_{\alpha,\beta}} t_1) \\
 &\xrightarrow{t_2} N_x \cos(\Omega_{C_{\alpha,\beta}} t_1) \cos(\Omega_N t_2) + N_y \cos(\Omega_{C_{\alpha,\beta}} t_1) \sin(\Omega_N t_2) \\
 &\xrightarrow{2\tau} 2H_z N_y \cos(\Omega_{C_{\alpha,\beta}} t_1) \cos(\Omega_N t_2) \\
 &\quad - 2H_z N_x \cos(\Omega_{C_{\alpha,\beta}} t_1) \sin(\Omega_N t_2)
 \end{aligned} \tag{5.79}$$

The delay δ is set to 11 ms according to Figure 5.11 and τ is set to $1/4 J_{NH} = 2.7$ ms. The coherence of the two FIDs obtained via the PEP scheme can be described by:

$$\begin{aligned}
 &H_x \cos(\Omega_{C_{\alpha,\beta}} t_1) \sin(\Omega_N t_2) - H_y \cos(\Omega_{C_{\alpha,\beta}} t_1) \cos(\Omega_N t_2) \\
 &H_x \cos(\Omega_{C_{\alpha,\beta}} t_1) \sin(\Omega_N t_2) + H_y \cos(\Omega_{C_{\alpha,\beta}} t_1) \cos(\Omega_N t_2)
 \end{aligned} \tag{5.80}$$

The coefficients that are used to optimize delays include: $n \times \sin(\pi J_{CH_n} \delta_1) \cos^{n-1}(\pi J_{CH_n} \delta_1)$, which are optimized for CH, CH₂, and CH₃ groups (Figure 5.10), and set $\tau_1 = 2.2$ ms; $\sin(\pi^1 J_{C^\alpha \beta H} \tau_1)$ is used to set $\delta_1 = 1.8$ ms [$1/(4 J_{C^\alpha \beta H})$]; T_1 is set to $1/(8 J_{C_\alpha C_\beta}) = 3.6$ ms; the delays τ_2 and δ are optimized to 11 ms according to Figure 5.11; and τ is set to $1/4 J_{NH} = 2.7$ ms.

5.4.5. CBCA(CO)NH

The 3D CBCA(CO)NH experiment correlates the chemical shifts of both C_{i-1}^α and C_{i-1}^β carbons with H_i^N and N_i . By correlating both C^α and C^β simultaneously, the degeneracy

of C^α –H resonances can be eliminated. The resonances of C^α and C^β provide information about the amino acid type of the preceding residue in addition to the sequential connectivity. The experiment is derived from CBCANH, utilizing a relayed COSY sequence to transfer C^β to C^α before the coherence is transferred to the amide C' spins:

$$H_{\alpha,\beta} \xrightarrow{J_{C\alpha\beta}H} C_{\alpha,\beta}(t_1) \xrightarrow{J_{C\alpha}C_\beta} C_\alpha \xrightarrow{J_{C\alpha}C'} C' \xrightarrow{J_{C'}N} N(t_2) \xrightarrow{J_{NH}} H(t_3) \quad (5.81)$$

The product operators representing the observable coherence throughout the transfers after the 90° $C^{\alpha\beta}$ pulse at the end of the t_1 evolution period in the CBCA(CO)NH pulse sequence (Figure 5.12) is the same as in CBCANH:

$$\begin{aligned} H_z &\xrightarrow{\frac{\pi}{2}H_x \rightarrow \tau_1 \rightarrow \pi(H_x + C_x^{\alpha,\beta}) \rightarrow \tau_1 \rightarrow \frac{\pi}{2}(H_y + C_x^{\alpha,\beta}) \rightarrow \delta_1} -C_x^{\alpha,\beta} \\ &\xrightarrow{t_1 \rightarrow 2T_1 \rightarrow \frac{\pi}{2}C_x^{\alpha,\beta}} \left(C_x^\alpha - 2C_y^\alpha C_z^\beta \right) \cos(\Omega_{C_{\alpha,\beta}} t_1) \end{aligned} \quad (5.82)$$

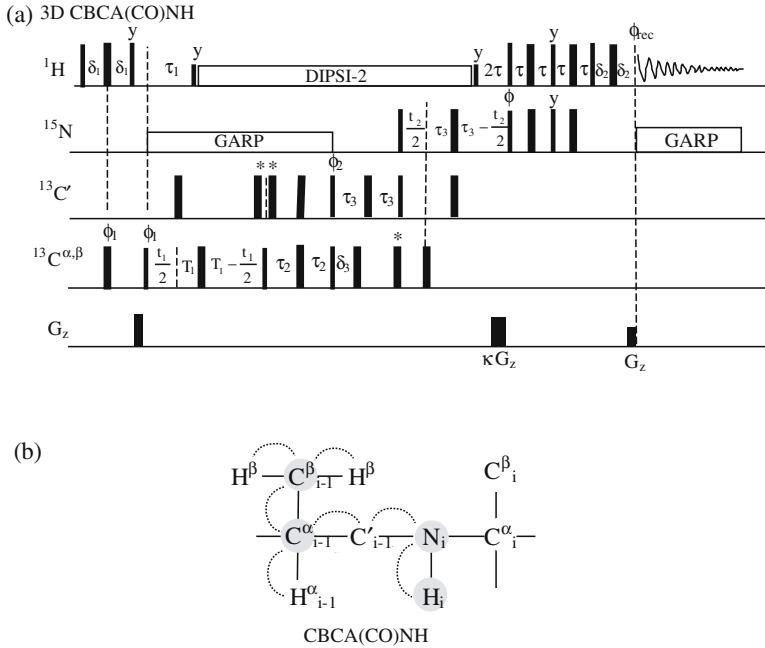


Figure 5.12. Pulse sequence of 3D CBCA(CO)NH. The magnetization starts from the H^α and H^β protons and is finally transferred to HN protons. The two C' 180° pulses labeled by * are used to compensate for the phase error introduced by the previous and subsequent off-resonance C' 180° pulses, respectively, while the C^α 180° pulse labeled by * is used to compensate for the phase error introduced by the previous off-resonance C^α 180° pulse. The phase cycles ϕ_1 and ϕ_2 are the same as in HNCO (Figure 5.2). The delays are set to $\delta_1 = 1.8$ ms, $\tau_1 = 2.2$ ms, $T_1 = 3.6$ ms, $\tau_2 = 3.5$ ms, $\delta_3 = 4.5$ ms, $\tau_3 = 13.5$ ms, $\tau = 2.7$ ms, and δ_2 equals the G_z gradient pulse length. (b) The dotted lines indicate the magnetization transfer pathways and the observed correlations are indicated by the shaded nuclei: H_i , N_i , to C_{i-1}^α , C_{i-1}^β , relayed via C_{i-1}' .

The time constant T_1 is set to $T_1 = 1/(8J_{C_\alpha C_\beta})$. The delay τ_1 is set to 1.8 ms and is optimized for $^1J_{C_\alpha\beta H}$ couplings and δ_1 is set to 2.2 ms to simultaneously optimize the CH_n coherence transfers of methine, methylene, and methyl groups (Figure 5.10). The gradient pulse after the 90° 1H pulse dephases all transverse magnetization. Only C^α magnetization terms, C_x^α and $2C_z^\alpha C_y^\beta$, will be transferred to C' in the following steps:

$$\begin{aligned} & \left(C_x^\alpha - 2C_y^\alpha C_z^\beta \right) \cos(\Omega_{C_{\alpha,\beta}} t_1) \xrightarrow{\tau_2 \rightarrow \pi(C_x^\alpha + C_x') \rightarrow \tau_2 \rightarrow 2\pi J_{C_\alpha C_\beta} \tau_2 \rightarrow 2\pi J_{C_\alpha C'} \tau_2} \\ & 2C_y^\alpha C_z' \cos(\Omega_{C_{\alpha,\beta}} t_1) \cos(2\pi J_{C_\alpha C_\beta} \tau_2) \sin(2\pi J_{C_\alpha C'} \tau_2) \\ & + 2C_y^\alpha C_z' \cos(\Omega_{C_{\alpha,\beta}} t_1) \sin(2\pi J_{C_\alpha C_\beta} \tau_2) \sin(2\pi J_{C_\alpha C'} \tau_2) \end{aligned} \quad (5.83)$$

in which the first term originates from C^α and the second term from C^β coherence (the term $-2C_y^\alpha C_z^\beta$). The delay τ_2 is optimized to 3.5 ms according to the coefficients $\cos(2\pi J_{C_\alpha C_\beta} \tau) \sin(2\pi J_{C_\alpha C'} \tau)$ and $\sin(2\pi J_{C_\alpha C_\beta} \tau) \sin(2\pi J_{C_\alpha C'} \tau)$ with $J_{C_\alpha C'} = 55$ Hz, and $J_{C_\alpha C_\beta} = 35$ Hz. The C^α 90°_x pulse gives coherence $2C_z^\alpha C_z'$ which is converted into $-2C_y' C_z^\alpha$ by the C' 90°_x pulse:

$$2C_y^\alpha C_z' \cos(\Omega_{C_{\alpha,\beta}} t_1) \xrightarrow{\frac{\pi}{2}(C_x^\alpha + C_x')} -2C_y' C_z^\alpha \cos(\Omega_{C_{\alpha,\beta}} t_1) \quad (5.84)$$

During the next period, the coherence evolves for $\delta_3 - (\tau_3 - \delta_3) + \tau_3 = 2\delta_3$ under the influence of $J_{C_\alpha C'}$, while the evolution caused by $J_{NC'}$ lasts for a period of $2\tau_3$:

$$\begin{aligned} & -2C_y' C_z^\alpha \cos(\Omega_{C_{\alpha,\beta}} t_1) \xrightarrow{2\delta_3} C_x' \cos(\Omega_{C_{\alpha,\beta}} t_1) \sin(2\pi J_{C_\alpha C'} \delta_3) \\ & \xrightarrow{\tau_3 \rightarrow \pi(N_x + C_x') \rightarrow \tau_3 \rightarrow \frac{\pi}{2}(N_x + C_x')} -2N_y C_z^\alpha \cos(\Omega_{C_{\alpha,\beta}} t_1) \\ & \sin(2\pi J_{C_\alpha C'} \delta_3) \sin(2\pi J_{NC'} \tau_3) \end{aligned} \quad (5.85)$$

The delay δ_3 is optimized to $1/(4J_{C_\alpha C'})$, which is approximately 4.5 ms, and τ_3 to $1/(4J_{NC'})$, approximately 13.5 ms. During t_2 constant evolution, the coherence evolves for $2\tau_3$ under the interaction of $J_{NC'}$:

$$\begin{aligned} & -2N_y C_z^\alpha \cos(\Omega_{C_{\alpha,\beta}} t_1) \xrightarrow{2\tau_3} N_x \cos(\Omega_{C_{\alpha,\beta}} t_1) \\ & \xrightarrow{t_2} N_x \cos(\Omega_{C_{\alpha,\beta}} t_1) \cos(\Omega_{N} t_2) + N_y \cos(\Omega_{C_{\alpha,\beta}} t_1) \sin(\Omega_{N} t_2) \\ & \xrightarrow{2\tau} 2H_z N_y \cos(\Omega_{C_{\alpha,\beta}} t_1) \cos(\Omega_{N} t_2) - 2H_z N_x \cos(\Omega_{C_{\alpha,\beta}} t_1) \sin(\Omega_{N} t_2) \end{aligned} \quad (5.86)$$

The delay τ_3 is chosen to optimize the $J_{NC'}$ coherence transfer as 12.5 ms, and τ is set to $1/(4J_{NH}) = 2.7$ ms for maximizing the NH coherence transfer. The magnetization is transferred back to protons and the two FIDs obtained via the PEP sequence for sensitivity

enhancement are given by:

$$H_x \cos(\Omega_{C_{\alpha,\beta}} t_1) \sin(\Omega_N t_2) - H_y \cos(\Omega_{C_{\alpha,\beta}} t_1) \cos(\Omega_N t_2) \quad (5.87)$$

$$H_x \cos(\Omega_{C_{\alpha,\beta}} t_1) \sin(\Omega_N t_2) + H_y \cos(\Omega_{C_{\alpha,\beta}} t_1) \cos(\Omega_N t_2) \quad (5.88)$$

In the same way as described earlier to rearrange the data by addition and subtraction, the final spectrum has a maximum gain in sensitivity by a factor of $\sqrt{2}$, which comes from the factor-two gain of signal intensity reduced by the increase of noise by a factor of $\sqrt{2}$. The delays and ^{13}C pulses for the experiment are set up as described in the figure legend.

5.5. EXPERIMENTS FOR SIDE-CHAIN ASSIGNMENT

5.5.1. HCCH–TOCSY

The HCCH–TOCSY experiment correlates all aliphatic ^1H and ^{13}C spins within residues, and is used to assign aliphatic ^1H and ^{13}C resonances and connect the side-chain chemical shifts with the backbone assignments. The experiment spreads a 2D TOCSY spectrum into a third or even fourth dimension to reduce signal overlapping. The magnetization originating at aliphatic ^1H is transferred to the directly attached ^{13}C via the one-bond scalar coupling ($^1J_{\text{CH}} \approx 140 \text{ Hz}$) after the evolution of the ^1H chemical shift during t_1 . The ^{13}C chemical shift evolves during t_2 before the ^{13}C magnetization is transferred further to the neighboring carbons via one-bond $^1J_{\text{CC}}$ ($30 \sim 40 \text{ Hz}$) during the isotropic mixing period. The ^{13}C magnetization is transferred to other ^{13}C spins within the spin system (amino acid residue) by isotropic mixing of ^{13}C spins via $^1J_{\text{CC}}$, which is more efficient than the ^1H isotropic mixing in the 2D TOCSY experiment via $^3J_{\text{HH}}$. Finally, the magnetization dispersed along the carbon side-chain is transferred to proton spins for detection. The transfer pathway for the pulse sequence is:

3D H(C)CH–TOCSY:

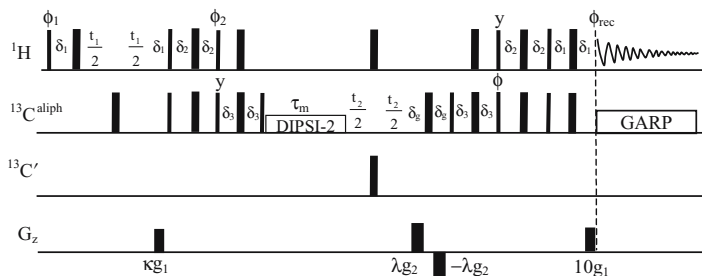
$$H_i(t_1) \xrightarrow{^1J_{\text{HC}} \approx 140 \text{ Hz}} C_i \xrightarrow{^1J_{C_i C_j} \approx 30 \sim 40 \text{ Hz (TOCSY)}} C_j(t_2) \xrightarrow{^1J_{\text{HC}} \approx 140 \text{ Hz}} H(t_3) \quad (5.89)$$

4D HCCH–TOCSY:

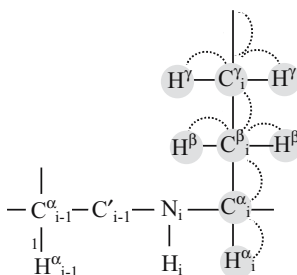
$$H_i(t_1) \xrightarrow{^1J_{\text{HC}} \approx 140 \text{ Hz}} C_i(t_2) \xrightarrow{^1J_{C_i C_j} \approx 30 \sim 40 \text{ Hz (TOCSY)}} C_j(t_3) \xrightarrow{^1J_{\text{HC}} \approx 140 \text{ Hz}} H(t_4) \quad (5.90)$$

Aliphatic proton TOCSY-type correlations of a given spin system are located at the ^{13}C 2D slices through all carbon frequencies within the spin system (same residue), whereas a ^1H 2D slice gives the total correlations between the ^1H and ^{13}C involved in the same spin system. As a result, 3D H(C)CH–TOCSY (Figure 5.13; Sattler *et al.*, 1995a,b) provides aliphatic ^1H and ^{13}C chemical shifts for the complete assignment of side-chain ^1H and ^{13}C resonances. Because the coherence is transferred via large coupling constants, the sensitivity of the experiment provides excellent sensitivity that can be further improved by a maximum factor of $2(\sqrt{2}\sqrt{2})$ utilizing double sensitivity enhancement after the t_1 and t_2 evolution periods. The sensitivity enhanced gradient pulse sequence also provides superior water suppression which makes it possible to obtain the spectra for side-chain ^1H and ^{13}C assignment with the same aqueous

(a) 3D H(C)CH-TOCSY



(b)



H(C)CH-TOCSY

Figure 5.13. Pulse sequence for 3D H(C)CH-TOCSY. All pulses are x phase including DIPSI-2, except $\phi_1 = x, -x$, $\phi_2 = y$, $\phi = y$ and $\phi_{\text{rec}} = x, -x$. Four FIDs are acquired with $\kappa = 1, -1, -1, 1$, $\lambda = 1, -1$, $\phi_2 = y, y, -y, -y$, and $\phi = y, -y$, and stored in different memory locations for the double sensitivity enhancement using both t_1 and t_2 coherences. Gradients are used as $g_2 = 18g_1$. $\delta_1 = 1.8$ ms, $\delta_2 = 0.8$ ms, $\delta_3 = 1.1$ ms, and δ_g equals the G_z gradient pulse length. (b) The observed correlations are between shaded nuclei.

samples used for the backbone assignment so that the ^2H effect on the chemical shifts of ^1H and ^{13}C can be avoided.

The description of the coherence transfer by product operators for the building blocks in the H(C)CH-TOCSY experiment (Figure 5.13) is given as follows, without considering the second sensitivity enhancement sequence. The initial magnetization of H^{aliph} is transferred to C^{aliph} by an HMQC-type sequence, during which the H^{aliph} chemical shift evolves for a period of t_1 , while the J_{CH} coupling evolves for a period of $2\delta_1(\delta_1 + \frac{1}{t_1} - \frac{1}{t_1} + \delta_1)$:

$$\text{H}_z \xrightarrow{\frac{\pi}{2}\text{H}_x} -\text{H}_y \quad (5.91)$$

$$\begin{aligned} -\text{H}_y &\xrightarrow{\delta_1 \rightarrow \pi\text{H}_x \rightarrow \frac{t_1}{2} \rightarrow \pi\text{C}_x \rightarrow \frac{t_1}{2} \rightarrow \delta_1} 2\text{H}_x\text{C}_z \sin(2\pi J_{\text{CH}}\delta_1) \cos(\Omega_{\text{H}}t_1) \\ &+ 2\text{H}_y\text{C}_z \sin(2\pi J_{\text{CH}}\delta_1) \sin(\Omega_{\text{H}}t_1) \end{aligned} \quad (5.92)$$

in which two terms will yield two components for the first sensitivity enhancement. The delay δ_1 is optimized for $^1J_{\text{CH}}$, which is set to $1/(4^1J_{\text{CH}}) = 1.8$ ms in the experiment. For simplicity, the terms of t_1 evolution are omitted temporarily from the equation and will be retrieved later.

For the first term of t_1 , the 90° ^1H and ^{13}C pulses transfer the coherence to C^{aliph} followed by sensitivity enhancement:

$$\begin{aligned}
 2\text{H}_x\text{C}_z &\xrightarrow{\frac{\pi}{2}(\text{H}_x+\text{C}_x)} -2\text{H}_x\text{C}_y \\
 &\xrightarrow{\delta_2 \rightarrow \pi(\text{H}_x+\text{C}_x) \rightarrow \delta_2} -2\text{H}_x\text{C}_y \xrightarrow{\frac{\pi}{2}(\text{H}_y+\text{C}_y)} 2\text{H}_z\text{C}_y \sin(2\pi J_{\text{CH}}\delta_2) \\
 &\xrightarrow{\delta_3 \rightarrow \pi(\text{H}_x+\text{C}_x) \rightarrow \delta_3 \rightarrow \frac{\pi}{2}\text{C}_x} -\text{C}_x \sin(2\pi J_{\text{CH}}\delta_2) \sin(2\pi n J_{\text{CH}}\delta_3)
 \end{aligned} \quad (5.93)$$

in which n is for different carbon multiplicities, CH_n . The multiple-quantum coherence ($2\text{H}_x\text{C}_y$) does not evolve under the influence of scalar coupling. The coefficients are different for different carbon multiplicities. Delay δ_2 is chosen as 0.8 ms approximated for both methylene and methyl carbon [the maximum transfer at $1/(8^1J_{\text{CH}})$ for methylene and $0.196/(2^1J_{\text{CH}})$ for methyl carbons] and δ_3 is set to 1.1 ms to optimize the coherence transfer simultaneously for all carbon multiplicities.

After the DIPSI-2 isotropic mixing pulse sequence, a portion of the C_x coherence is transferred to neighboring carbons throughout the spin system:

$$-\text{C}_x \xrightarrow{\tau_m} -\sum_k^K \text{C}_x^k \quad (5.94)$$

During mixing time τ_m , the in-phase C_x magnetization is transferred to neighbor carbons C_x^k within residues via J_{CC} coupling. After retrieving the t_1 , the above coherence becomes:

$$\begin{aligned}
 -\sum_k^K \text{C}_x^k \cos(\Omega_{\text{H}}t_1) &\xrightarrow{\frac{1}{2}t_2 \rightarrow \pi(\text{C}_x) \rightarrow \frac{1}{2}t_2} -\sum_k^K \text{C}_x^k \cos(\Omega_{\text{H}}t_1) \cos(\Omega_{\text{C}^k}t_2) \\
 &\quad + \sum_k^K \text{C}_y^k \cos(\Omega_{\text{H}}t_1) \sin(\Omega_{\text{C}^k}t_2)
 \end{aligned} \quad (5.95)$$

The 180° $\text{C}_x^{\text{aliph}}$ pulse inverts the coherence and the gradient echo dephases any coherence generated due to imperfect refocusing by the 180° pulse. The isotropic mixing period is usually set to 25 ~ 30 ms with a field strength of ~8 kHz ($\text{pw}_{90} = \sim 30 \mu\text{s}$).

The two terms produced by t_2 evolution are used to obtain an additional set of FIDs by the second PEP sequence, resulting in a set of four FIDs to be recorded and stored in separated memory locations. The evolution of the first t_2 term throughout the remaining sequence is given by:

$$\begin{aligned}
 -\text{C}_x^k &\xrightarrow{\frac{\pi}{2}\text{C}_x \rightarrow \delta_3 \rightarrow \pi(\text{H}_x+\text{C}_x) \rightarrow \delta_3} -2\text{H}_z\text{C}_y^k \xrightarrow{\frac{\pi}{2}(\text{H}_y+\text{C}_y)} -2\text{H}_x\text{C}_y^k \\
 &\xrightarrow{\delta_2 \rightarrow \pi(\text{H}_x+\text{C}_x) \rightarrow \delta_2} -2\text{H}_x\text{C}_y^k \xrightarrow{\frac{\pi}{2}(\text{H}_x+\text{C}_x)} -2\text{H}_x\text{C}_z^k \\
 &\xrightarrow{\delta \rightarrow \pi(\text{H}_x+\text{C}_x) \rightarrow \delta} \text{H}_y
 \end{aligned} \quad (5.96)$$

After bringing in the coefficients of t_1 and t_2 , the observable magnetization from the first t_1 term with the first t_2 term is given by:

$$\sum_k^K H_y \cos(\Omega_H t_1) \cos(\Omega_{C^k} t_2) \quad (5.97)$$

The second t_1 term in Equation (5.92) throughout the pulse sequence can be described as:

$$2H_x C_z \cos(\Omega_H t_1) + 2H_y C_z \sin(\Omega_H t_1) \quad (5.98)$$

$$\begin{aligned} 2H_y C_z &\xrightarrow{\frac{\pi}{2}(H_x+C_x)} -2H_z C_y \xrightarrow{\delta_2 \rightarrow \pi(H_x+C_x) \rightarrow \delta_2} C_x \xrightarrow{\frac{\pi}{2}(H_y+C_y)} -C_z \\ &\xrightarrow{\delta_3 \rightarrow \pi(H_x+C_x) \rightarrow \delta_3} C_z \xrightarrow{\frac{\pi}{2}C_x} -C_y \xrightarrow{\tau_m} -\sum_k^K C_y^k \end{aligned} \quad (5.99)$$

$$\begin{aligned} -\sum_k^K C_y^k \cos(\Omega_H t_1) &\xrightarrow{\frac{1}{2}t_2 \rightarrow \pi(C'_x+N) \rightarrow \frac{1}{2}t_2} -\sum_k^K C_y^k \sin(\Omega_H t_1) \cos(\Omega_{C^k} t_2) \\ &\quad + \sum_k^K C_x^k \sin(\Omega_H t_1) \sin(\Omega_{C^k} t_2) \end{aligned} \quad (5.100)$$

From the first t_2 term of the above equation, the coherence is transferred as:

$$\begin{aligned} -C_y^k &\xrightarrow{\frac{\pi}{2}C_x} -C_z^k \xrightarrow{\delta_3 \rightarrow \pi(H_x+C_x) \rightarrow \delta_3} C_z^k \xrightarrow{\frac{\pi}{2}(H_y+C_y)} C_x^k \\ &\xrightarrow{\delta_2 \rightarrow \pi(H_x+C_x) \rightarrow \delta_2} 2H_z C_y^k \xrightarrow{\frac{\pi}{2}(H_x+C_x)} -2H_y C_z^k \\ &\xrightarrow{\delta \rightarrow \pi(H_x+C_x) \rightarrow \delta} H_x \end{aligned} \quad (5.101)$$

After bringing in the coefficients of t_1 and t_2 , the observable magnetization from the second t_1 term with the first t_2 term is given by:

$$\sum_k^K H_x \sin(\Omega_H t_1) \cos(\Omega_{C^k} t_2) \quad (5.102)$$

Using the result for the second t_1 and first t_2 [Equation (5.101)] during the PEP sequence:

$$-C_y^k \xrightarrow{\text{PEP}} H_x \quad (5.103)$$

the term from the first t_1 and the second t_2 in Equation (5.95) gives:

$$C_y^k \xrightarrow{\text{PEP}} -\sum_k^K H_x \cos(\Omega_H t_1) \sin(\Omega_{C^k} t_2) \quad (5.104)$$

Similarly, the term of the second t_1 and the second t_2 in Equation (5.100) after the PEP sequence is given by:

$$C_x^k \xrightarrow{\text{PEP}} - \sum_k^K H_y \sin(\Omega_H t_1) \sin(\Omega_{C^k} t_2) \quad (5.105)$$

The coherence transfers for the four terms generated after t_2 evolution throughout the PEP sequence can be summarized as:

$$t_1 \begin{cases} 2H_x C_z \xrightarrow{t_2} \begin{cases} -C_x^k \rightarrow \sum_k^K H_y \cos(\Omega_H t_1) \cos(\Omega_{C^k} t_2) \\ C_y^k \rightarrow -\sum_k^K H_x \cos(\Omega_H t_1) \sin(\Omega_{C^k} t_2) \end{cases} \\ 2H_y C_z \xrightarrow{t_2} \begin{cases} -C_y^k \rightarrow \sum_k^K H_x \sin(\Omega_H t_1) \cos(\Omega_{C^k} t_2) \\ C_x^k \rightarrow -\sum_k^K H_y \sin(\Omega_H t_1) \sin(\Omega_{C^k} t_2) \end{cases} \end{cases} \quad (5.106)$$

Therefore, the product operators for the first FID are given by:

$$\begin{aligned} & \sum_k^K [H_y \cos(\Omega_H t_1) \cos(\Omega_{C^k} t_2) - H_x \cos(\Omega_H t_1) \sin(\Omega_{C^k} t_2) \\ & + H_x \sin(\Omega_H t_1) \cos(\Omega_{C^k} t_2) - H_y \sin(\Omega_H t_1) \sin(\Omega_{C^k} t_2)] \end{aligned} \quad (5.107)$$

The second FID is obtained by inverting the phase ϕ and the first three gradients. The C_x^k coherence obtained after t_2 evolution is not affected by the phase inversion, while C_y^k coherence changes sign. Consequently, the second FID is given by:

$$\begin{aligned} & \sum_k^K [H_y \cos(\Omega_H t_1) \cos(\Omega_{C^k} t_2) + H_x \cos(\Omega_H t_1) \sin(\Omega_{C^k} t_2) \\ & - H_x \sin(\Omega_H t_1) \cos(\Omega_{C^k} t_2) - H_y \sin(\Omega_H t_1) \sin(\Omega_{C^k} t_2)] \end{aligned} \quad (5.108)$$

The third FID is acquired by inverting the phase of ϕ_1 , which changes the sign of the first t_1 term:

$$\begin{aligned} & \sum_k^K [-H_y \cos(\Omega_H t_1) \cos(\Omega_{C^k} t_2) + H_x \cos(\Omega_H t_1) \sin(\Omega_{C^k} t_2) \\ & + H_x \sin(\Omega_H t_1) \cos(\Omega_{C^k} t_2) - H_y \sin(\Omega_H t_1) \sin(\Omega_{C^k} t_2)] \end{aligned} \quad (5.109)$$

The last FID is acquired with inverting both phases of ϕ_1 and ϕ , which has a form of:

$$\begin{aligned} & \sum_k^K [-H_y \cos(\Omega_H t_1) \cos(\Omega_{C^k} t_2) - H_x \cos(\Omega_H t_1) \sin(\Omega_{C^k} t_2) \\ & - H_x \sin(\Omega_H t_1) \cos(\Omega_{C^k} t_2) - H_y \sin(\Omega_H t_1) \sin(\Omega_{C^k} t_2)] \end{aligned} \quad (5.110)$$

The four FIDs are recorded and stored separately. The combinations of the data yield four data sets that can be transformed to four spectra and combined to a single spectrum with pure phase in all three dimensions. A maximum sensitivity enhancement by a factor of 2 can be obtained in the combined spectrum:

$$\begin{aligned}
 \text{FID}_1 + \text{FID}_2 - \text{FID}_3 - \text{FID}_4 &= 4H_y \cos(\Omega_H t_1) \cos(\Omega_C^k t_2) \\
 -\text{FID}_1 + \text{FID}_2 + \text{FID}_3 - \text{FID}_4 &= 4H_x \sin(\Omega_H t_1) \cos(\Omega_C^k t_2) \\
 \text{FID}_1 - \text{FID}_2 + \text{FID}_3 - \text{FID}_4 &= 4H_x \cos(\Omega_H t_1) \sin(\Omega_C^k t_2) \\
 -\text{FID}_1 - \text{FID}_2 - \text{FID}_3 - \text{FID}_4 &= 4H_y \sin(\Omega_H t_1) \sin(\Omega_C^k t_2)
 \end{aligned} \tag{5.111}$$

5.6. 3D ISOTOPE-EDITED EXPERIMENTS

5.6.1. ^{15}N -HSQC-NOESY

The signal overlapping of ^1H spins becomes more severe with an increase in molecular size. The 3D heteronuclear-edited experiments resolve the overlapped ^1H resonances over the chemical shift frequencies of the directly attached heteronuclei (^{15}N and/or ^{13}C), resulting in a significant increase in resolution in the ^1H dimensions. The simplest way to form a 3D pulse sequence is to combine two 2D pulse sequences. 3D NOESY-HSQC is formed by combining an HSQC with a NOESY after removing the acquisition period of the NOESY and the preparation period of the HSQC (Figure 6.7b; Marion *et al.*, 1989). After the evolution of ^1H chemical shifts, the magnetization is transferred to vicinal protons by cross relaxation during the NOESY mixing period, τ_m . The scalar coupling of ^{15}N to ^1H is refocused by the ^{15}N 180° pulses in the middle of the t_1 evolution of the ^1H chemical shifts. In the following step, the magnetization of the amide proton spins is transferred to ^{15}N and then back to amide protons after the evolution of ^{15}N chemical shifts in the same pathway as in the HSQC experiment. The PEP scheme is used for sensitivity enhancement:

$$H(t_1) \xrightarrow{\text{NOE}} H \xrightarrow{J_{\text{HN}}} N(t_2) \xrightarrow{J_{\text{HN}}} H(t_3) \tag{5.112}$$

The description of the coherence transfer by the product operators is given by:

$$\begin{aligned}
 H_z &\xrightarrow{\frac{\pi}{2} H_x \rightarrow t_1 \rightarrow \pi N_x \rightarrow t_1} -H_y \cos(\Omega_H t_1) + H_x \sin(\Omega_H t_1) \\
 &\xrightarrow{\frac{\pi}{2} H_x} -H_z \cos(\Omega_H t_1) + H_x \sin(\Omega_H t_1) \\
 &\xrightarrow{\tau_m} -H_z \cos(\Omega_H t_1)
 \end{aligned} \tag{5.113}$$

The transverse magnetization is removed by the gradient pulse:

$$\begin{aligned}
 -H_z \cos(\Omega_H t_1) &\xrightarrow{\frac{\pi}{2} H_x} H_y \cos(\Omega_H t_1) \\
 &\xrightarrow{\tau \rightarrow \pi(H_x + C_x^{\alpha, \beta}) \rightarrow \tau \rightarrow \frac{\pi}{2} H_y} 2H_z N_z \cos(\Omega_H t_1) \sin(2\pi J_{\text{HN}} \tau)
 \end{aligned} \tag{5.114}$$

The delay t is optimized to $1/(4J_{\text{HN}})$, which is approximately 2.7 ms, so that the coefficient equals one. The water magnetization is brought to the transverse plane by the flip-back selective pulse and consequently destroyed by the gradient pulse:

$$2H_z N_z \cos(\Omega_{\text{H}t_1}) \xrightarrow{\frac{\pi}{2} N_x} -2H_z N_y \cos(\Omega_{\text{H}t_1}) \\ \xrightarrow{t_2} -2H_z N_y \cos(\Omega_{\text{H}t_1}) \cos(\Omega_{\text{H}t_2}) + 2H_z N_x \cos(\Omega_{\text{H}t_1}) \sin(\Omega_{\text{H}t_2}) \quad (5.115)$$

The two terms will be used to achieve sensitivity enhancement by the PEP sequence. The gradient echo scheme before the beginning of PEP sensitivity enhancement is used to select the desired coherence pathway and to invert the coherence order for the PEP sequence. From the results of PEP in the HNCO sequence, the two FIDs after PEP are given by:

$$H_y \cos(\Omega_{\text{C}t_1}) \cos(\Omega_{\text{N}t_2}) - H_x \cos(\Omega_{\text{C}t_1}) \sin(\Omega_{\text{N}t_2}) \quad (5.116)$$

$$H_y \cos(\Omega_{\text{C}t_1}) \cos(\Omega_{\text{N}t_2}) + H_x \cos(\Omega_{\text{C}t_1}) \sin(\Omega_{\text{N}t_2}) \quad (5.117)$$

The two FIDs are recorded separately and stored in different memory locations. The combinations of the two FIDs yield two sets of data:

$$2H_y \cos(\Omega_{\text{C}t_1}) \cos(\Omega_{\text{N}t_2}) \quad (5.118)$$

$$2H_x \cos(\Omega_{\text{C}t_1}) \sin(\Omega_{\text{N}t_2}) \quad (5.119)$$

After Fourier transformation, the two spectra are added to form a single spectrum with enhanced sensitivity.

5.7. SEQUENCE-SPECIFIC RESONANCE ASSIGNMENTS OF PROTEINS

5.7.1. Assignments Using ^{15}N Labeled Proteins

Through-bond correlation via ^1H – ^1H scalar couplings can be observed only for protons separated by two or three bonds since long-range ^1H – ^1H scalar couplings are usually negligibly weak. Therefore, correlation spectra via ^1H – ^1H scalar couplings do not give correlations between H_i^{N} and H_{i+1}^{α} . The observed cross-peaks are the correlations between protons within the same amino acid residue, or spin system. Each ^1H spin system corresponds to an amino acid residue. Nuclei with different chemical environments have different chemical shift ranges. Chemical shifts for H^{N} , H^{α} , and aliphatic side-chain protons have characteristic ranges, with H^{N} resonances between 7–10 ppm, H^{α} 3.5–6 ppm, and H^{aliph} 1–3.5 ppm. For the majority of residues, the type of protons (H^{N} , H^{α} , H^{aliph}) are readily identified when their spin systems are located in the spectrum. However, it is troublesome to obtain complete ^1H assignments for a protein with more than 50 residues because the resonance overlap becomes severe.

To reduce resonance overlap, the magnetization of protons with resonances in the crowded chemical shift regions (H^{α} , H^{aliph}) is observed in (or transferred to) the less crowded H^{N} region using the TOCSY experiment. In the TOCSY spectrum, each ^1H spin system is observed along the resonance of the backbone H^{N} in the fingerprint region defined by H^{N} resonances in the F_2 dimension and those of H^{α} and H^{aliph} in the F_1 dimension.

The connectivity between adjacent residues is established by the NOE cross-peaks of H_i^N to H_{i+1}^α in a NOESY or ROESY spectrum. The cross-peaks from H_i^N to H_{i+1}^N can also yield sequential connectivities. To improve the spectral resolution and reduce the resonance overlap, 1H correlations in the fingerprint region of TOCSY or NOESY can be expanded along the ^{15}N frequency using an ^{15}N edited TOCSY or NOESY (Marion *et al.*, 1989; Muhandiram *et al.*, 1993). Correlations between amide 1H – ^{15}N are observed by HSQC. The HSQC sequence can be incorporated into the experiment either before or after TOCSY or NOESY sequence. The advantage of ^{15}N edited experiments is that they retain sufficient resolution in the 1H – 1H correlation plane. A typical assignment involves identifying spin systems at each ^{15}N frequency slice, assigning the resonances of the spin systems, and categorizing the spin systems to classes of amino acid residues based on the spin coupling topology. For example, Ile and Leu will belong to the same category because their spin systems have a similar coupling topology. Several amino acid residues have unique spin systems such as Gly, Ala, Val, Thr. It is always helpful to know the chemical shifts and spin topology of the above unique residues when identifying spin systems. It should be noted that proline does not have a spin system starting at an amide proton because of the absence of H^N . The total number of spin systems should match or be close to the number of amino acid residues minus the number of prolines. The next stage is to extend the sequential assignment from the starting amino acid residues to both directions in the sequence via NOE connectivities of H_i^N to H_{i+1}^α and/or to H_{i+1}^β . Suitable starting residues may be selected at Gly, Ala, or Val because they have unique sets of chemical shifts and are easily identified in the TOCSY spectrum. The ambiguous area is where long range H^N – H^α NOEs exist such as in the case of β sheets. The observed NOE may arise from nonsequential residues due to secondary or tertiary structure rather than the sequential connectivity. Usually an HSQC experiment is carried out first to examine the dispersion of amide 1H and ^{15}N chemical shifts. If the degeneracy of the $^1H/^{15}N$ pair is observed, it may be helpful to acquire data at two temperatures since H^N chemical shifts are sensitive to a change of temperature. When the temperature is changed, for example, by $10^\circ C$, the chemical shifts of degenerate H^N protons will move away from each other. As a result, the overlapped spin systems are resolved in the TOCSY spectrum.

5.7.2. Sequence-Specific Assignment Using Doubly Labeled Proteins

Backbone H^N , N , C^α , C' resonances are assigned by analyzing 3D HNCO, HNCA, HN(CA)CO, and HN(CO)CA experiments. HNCO and HN(CO)CA experiments provide single sets of correlations between $(H,N)_i$ and C'_{i-1} , and between $(H,N)_i$ and C^α_{i-1} , respectively, whereas HNCA and HN(CA)CO give rise to correlations both within the residues and to the preceding residues: $(H,N, C^\alpha)_i$, and $(H,N)_i, C^\alpha_{i-1}$ for HNCA, $(H, N, C')_i$ and $(H,N)_i, C'_{i-1}$ for HN(CA)CO experiments, because of the compatible size of scalar couplings $^1J_{NC\alpha}$ and $^2J_{NC\alpha}$. In principle, the four experiments will provide complete information for backbone assignments. However, since the experiments rely on the correlations of $(H, N)_i$, the degeneracy of the pair will cause ambiguities in the chemical shift assignment of C^α and C' . Hence, the degeneracy of H, N is usually inspected in an HSQC experiment before setting up the 3D experiments. If it exists, the degeneracy of H, N can be bypassed by the correlation between C'_{i-1} and C^α_i in 4D HNCO $_{i-1}$ CA $_i$ or 3D H(N)CO $_{i-1}$ CA $_i$ (Konrat *et al.*, 1999) so that the sequential assignment can be extended. An alternative is to move the H^N chemical shifts by lowering the temperature if the solubility of the sample is allowed.

Once the complete assignment of backbone nuclei is achieved, they can be extended to C^β by a pair of 3D experiments, CBCA(CO)NH and CBCANH, which correlate the chemical shifts of H_i^N , N_i with C_{i-1}^α , C_{i-1}^β and with C_i^α , C_i^β , C_{i-1}^α , and C_{i-1}^β , respectively. Since resonances of the backbone nuclei have been assigned previously, the assignment of C^β is relatively straightforward. The final stage of the assignment focuses on the aliphatic side-chain carbons and protons using a 3D or 4D HCCH-TOCSY and a 3D ^{15}N edited TOCSY. The HCCH-TOCSY is much more sensitive than the ^{15}N edited TOCSY because it utilizes the large $^1J_{\text{CC}}$ scalar coupling to transfer magnetization along the side-chain rather than relying on the $^3J_{\text{HH}}$ coupling as in the case of ^{15}N edited experiments. Each cross-peak of a 3D HCCH-TOCSY correlates the chemical shifts of H_i , H_j , and C_j for a spin system of $H_iC_i - \dots - H_jC_j$. The chemical shifts of aliphatic side-chain protons can be located at all resonances of side-chain carbons involved in the same spin system. The chemical shifts of the side-chain carbons are obtained by tracing their correlations with the proton spin system. The cross-peaks of a 4D HCCH-TOCSY correlate all four protons and carbons, H_i , C_i , H_j , and C_j , in the spin system. Therefore, each cross-peak provides two proton and two carbon frequencies. By now, the resonance assignments are complete and are ready to be used to identify NOE cross-peaks for structural calculations.

5.8. ASSIGNMENT OF NOE CROSS-PEAKS

After the complete assignment of backbone and side-chain resonances, the connectivities among the protons are readily assigned using a 4D ^{13}C - ^{13}C NOESY. In the initial stage of the assignment, usually, only a fraction of the total NOESY cross-peaks can be assigned unambiguously, because of chemical shift degeneracy and inconsistency in some extent of the NOESY cross-peak positions compared to those obtained by resonance assignment. Additional NOESY cross-peaks are assigned during the iterative steps of the structure calculation (see Chapter 7).

QUESTIONS

- 5.1. What is a PEP sequence used for? And how is it achieved?
- 5.2. Why is it necessary to obtain the resonance assignments?
- 5.3. What is the IPAP-HSQC experiment used for and how are the in-phase and anti-phase doublets generated by the pulse sequence?
- 5.4. What is an “out and back” experiment and how is this type of experiment named?
- 5.5. Why are the correlations of H_i^N and N_i with both C_i^α and C_{i-1}^α observed in the HNCA experiment but the correlations of H_i^N and N_i with C_i^α are not present in the HNCO experiment?

- 5.6. The ^1H sequence element “ 2τ -DIPSI-2” is present in many 3D triple-resonance experiments. What is this sequence used for and how is the delay τ set?
- 5.7. What are the coefficients used to optimize the delay (shown in Figure 5.10) for different carbon multiplicities?
- 5.8. Why do C^α cross-peaks in the CBCANH experiment have an opposite sign to C^β cross-peaks?

REFERENCES

- Akke, M., P. Carr, and A.G. Palmer III, *J. Magn. Reson.* **B104**, 298 (1994).
- Bax, A., G.M. Clore, and A.M. Gronenborn, *J. Magn. Reson.* **88**, 425 (1990a).
- Bax, A., M. Ikura, L.E. Kay, D.A. Torchia, and R. Tschudin, *J. Magn. Reson.* **86**, 304 (1990b).
- Bodenhausen, G. and D.J. Ruben, *Chem. Phys. Lett.* **69**, 185 (1980).
- Cavanagh, J., A.G. Palmer III, P.E. Wright, and M. Rance, *J. Magn. Reson.* **91**, 429 (1991).
- Cavanagh, J. and M. Rance, *Annu. Rep. NMR Spectrosc.* **27**, 1(1993).
- Clubb, R.T., V. Thanabal, and G. Wagner, *J. Magn. Reson.* **97**, 213 (1992).
- Coy, M.A. and L. Mueller, *J. Magn. Reson.* **A101**, 122 (1993).
- Delaglio, F., S. Grzesiek, G.W. Vuister, G. Zhu, J. Pfeifer, and A. Bax, “NMRPipe: a multidimensional spectral processing system based on UNIX pipes”, *J. Biomol. NMR.* **6**, 277–293 (1995).
- Delaglio, F., S. Grzesiek, G.W. Vuister, G. Zhu, J. Pfeifer, and A. Bax, <http://spin.niddk.nih.gov/bax/software/NMRPipe/> (2004).
- Emsley, L. and G. Bodenhausen, *Chem. Phys. Lett.* **165**, 469 (1990).
- Engelke, J. and H. Rüterjans, *J. Magn. Reson.* **B109**, 318 (1995).
- Ernst, R.R., G. Bodenhausen, and A. Wokaun, *The Principles of Nuclear Magnetic Resonance in One and Two Dimensions*, Oxford University Press, New York (1987).
- Fesik, S.W., H.L. Eaton, E.T. Olejniczak, E.R.P. Zuiderweg, L.P. McIntosh, and F.W. Dahlquist, *J. Am. Chem. Soc.* **112**, 886 (1990).
- Geen, H. and R. Freeman, *J. Magn. Reson.* **93**, 93 (1991).
- Gerald, R., T. Bernhard, U. Haegberlen, J. Rendell, and S. Opella, *J. Am. Chem. Soc.* **115**, 777–782 (1993).
- Grzesiek, S. and A. Bax, *J. Magn. Reson.* **99**, 201 (1992a).
- Grzesiek, S. and A. Bax, *J. Am. Chem. Soc.* **114**, 6291 (1992b).
- Grzesiek, S. and A. Bax, *J. Mol. Biol.* **287**, 569 (1992c).
- Grzesiek, S. and A. Bax, *J. Am. Chem. Soc.* **115**, 12593 (1993).
- Grzesiek, S., J. Anglister, and A. Bax, *J. Magn. Reson.* **B101**, 114 (1993).
- Hurd, R.E. and B.K. John, *J. Magn. Reson.* **91**, 648 (1991).
- Ikura, M., L.E. Kay, and A. Bax, *Biochemistry* **29**, 4659 (1990a).
- Ikura, M., D. Marion, L.E. Kay, *et al. Biochem. Pharmacol.* **40**, 153 (1990b).
- Johnson, B.A., <http://onemoonscientific.com/nmrview/> (2004).
- Kay, L.E., M. Ikura, R. Tschudin, and A. Bax, *J. Magn. Reson.* **89**, 496 (1990).
- Kay, L.E., M. Ikura, G. Zhu, and A. Bax, *J. Magn. Reson.* **91**, 422 (1991).
- Kay, L.E., P. Keifer, and T. Saarinen, *J. Am. Chem. Soc.* **114**, 10663 (1992).
- Kay, L. E., G.Y. Xu, and T. Yamazaki, *J. Magn. Reson.* **A109**, 129 (1994).
- Konrat, R., D. Yang, and L.E. Kay, *J. Biomol. NMR* **15**, 309 (1999).
- Lyons, B.A. and G.T. Montelione, *J. Magn. Reson.* **B101**, 206 (1993).
- Logan, T.M., E.T. Olejniczak, R.X. Xu, and S.W. Fesik, *J. Biomol. NMR* **3**, 225 (1993).
- Majumdar, A., H. Wang, R.C. Morshauser, and E.R.P. Zuiderweg, *J. Biomol. NMR* **3**, 387 (1993).

- Marion, D., L.E. Kay, S.W. Sparks, D.A. Torchia, and A. Bax, *J. Am. Chem.* **B103**, 203 (1989).
- Matsuo, H., E. Kupce, H. Li, and G. Wagner, *J. Magn. Reson.* **B113**, 91 (1996).
- McCoy, M., *J. Magn. Reson.* **B107**, 270 (1995).
- Montelione, G.T., B.A. Lyons, S.D. Emerson, and M. Tashiro, *J. Am. Chem. Soc.* **114**, 10974 (1992).
- Mueller, L., *J. Am. Chem. Soc.* **101**, 4481 (1979).
- Muhandiram, D.R., G.Y. Xu, and L.E. Kay, *J. Biomol. NMR* **3**, 463 (1993).
- Muhandiram, D.R. and L.E. Kay, *J. Magn. Reson.* **B103**, 203 (1994).
- Olejnyczak, E.T., R.X. Xu, and S.W. Fesik, *J. Biomol. NMR* **2**, 655 (1992).
- Ottiger, M., F. Delaglio, and A. Bax, *J. Magn. Reson.* **131**, 373 (1998).
- Palmer III, A.G., J. Cavanagh, P.E. Wright, and M. Rance, *J. Magn. Reson.* **91**, 429 (1991).
- Pervushin, K., R. Riek, G. Wider, and K. Wüthrich, *Proc. Natl. Acad. Sci. USA* **96**, 9607–9612 (1999).
- Pervushin, K., R. Riek, G. Wider, and K. Wüthrich, *Proc. Natl. Acad. Sci. USA* **94**, 12366 (1997).
- Sattler, M., P. Schmidt, J. Schleucher, O. Schedletsky, S.J. Glaser, and C. Griesinger, *J. Magn. Reson.* **B108**, 235 (1995a).
- Sattler, M., M. Schwedinger, J. Schleucher, and C. Griesinger, *J. Biomol. NMR* **6**, 11 (1995b).
- Schleucher, J., M.G. Schwendinger, M. Sattler, P. Schmidt, S.J. Glaser, O.W. Sørensen and C. Griesinger, *J. Biomol. NMR* **4**, 301 (1994).
- Sørensen, O.W., G.W. Eich, M.H. Levitt, G. Bodenhausen, and R.R. Ernst, *Prog. Nucl. Magn. Reson. Spectrosc.* **16**, 163 (1983).
- Teng, Q. and T.A. Cross, *J. Magn. Reson.* **85**, 439 (1989).